Ore Geology Reviews 72 (2016) 323–342

Contents lists available at ScienceDirect

Ore Geology Reviews

journal homepage: www.elsevier.com/locate/oregeorev

Eocene K-rich adakitic rocks in the Central Iran: Implications for evaluating its Cu–Au–Mo metallogenic potential

Jamshid Ahmadian [a,*], Fatemeh Sarjoughian [b], David Lentz [c], Amir Esna-Ashari [a], Mamoru Murata [d], Hiroaki Ozawa [d]

[a] Department of Geology, Payame Noor University, PO Box 19395-3697 Iran
[b] Department of Earth Sciences, Faculty of Sciences, University of Kurdistan, Iran
[c] Department of Earth Sciences, University of New Brunswick, Fredericton, NB E3B 5A3, Canada
[d] Department of Geosciences, Naruto University of Education, 748 Nakashima, Takashima 772-8502, Japan

ARTICLE INFO

Article history:
Received 17 February 2015
Received in revised form 20 July 2015
Accepted 21 July 2015
Available online 26 July 2015

Keywords:
Adakite
Delamination
Kal-e-Kafi
Iran

ABSTRACT

The Kal-e-Kafi intrusive complex is located in the Central Iran magmatic zone and includes a series of granitoid rocks ranging in composition from gabbro to granite. These granitoids show some affinities with adakites, e.g., high Sr/Y and La/Yb ratios coupled with low Yb and Y, enrichment in LREE and LILE with no Eu anomalies, similar to products from all of which are compatible with derivation from slab melting. However, relatively their low $\varepsilon Nd_{(t)}$ values (0.21 to 2.35) and higher $^{87}Sr/^{86}Sr_i$ (0.7041–0.7044) are inconsistent with an origin by slab melting with these rocks also showing shoshonitic affinities, with high K_2O/Na_2O ratios. Geochemical characteristics indicate that the Kal-e-Kafi intrusive complex was probably derived by the partial melting of delaminated lower crust, at pressures equivalent to crustal thicknesses of >40 km, generated near the boundary between garnet-bearing amphibolite or amphibole-bearing eclogite melting. Moreover, the Kal-e-Kafi adakitic magmas must have interacted with the surrounding metasomatized mantle peridotite during their ascent, which elevated not only their MgO, Cr, and Ni contents, but also the oxygen fugacity (fO_2) of the magma. The high fO_2 could have induced oxidation of metallic sulfides in the mantle resulting in the mobilization of chalcophile elements, which are required to produce porphyry Cu (Au and Mo) mineralization.

1. Introduction

Adakitic rocks, initially identified on Adak Island in the Central Aleutians, have high MgO values, are rich in large ion lithophile elements (LILE), and have high Sr/Y ratios (Kay, 1978). Defant and Drummond (1990) used the term adakite for intermediate-acid and Na-rich igneous rocks, which are thought to be derived by partial melting of subducted young oceanic crust (≤25 Ma). They are geochemically characterized by $SiO_2 \geq 56$ wt.%, $Al_2O_3 \geq 15$ wt.% (rarely lower), usually MgO < 3 wt.% (rarely above 6 wt.% MgO), extremely high light rare element (LREE) concentrations and very low Y and heavy rare element (HREE) concentrations (e.g., Y < 18 ppm, Yb < 1.8 ppm), very high Sr/Y ratios (>40) and La/Yb ratios (>9), no obvious negative Eu anomaly, and $^{87}Sr/^{87}Sr$ usually <0.7040, but high Nd isotopic compositions (see Castillo, 2006). As a matter of fact, the rocks described by Kay (1978) at Adak are not considered to be adakites using the definition of by Defant and Drummond (1990).

Martin and Moyen (2003) showed that there are two main compositional groups defined, based on their silica content as high-SiO_2 adakites (HSA; $SiO_2 > 60$ wt.%) and low-SiO_2 adakites (LSA; $SiO_2 < 60$ wt.%). HSA, corresponding to the rocks originally described by Defant and Drummond (1990), are formed by partial melting of metabasalts, in the field of garnet stability and having relatively elevated Nb/Ta (14 ± 4), probably corresponding to a rutile-bearing residuum. It was also initially believed that adakite only occurs in young convergent margins (<25 Ma) and thus still hot oceanic slabs are being subducted, consistent with results of combined partial melting models for subducted basaltic crust (Castillo, 2006). LSA, more closely related to high-$Mg^{\#}$ andesites, which encompasses rocks with SiO_2 values as low as 50% (adakites from Adak island), but usually have $50\% < SiO_2 < 60\%$, and correlatively high contents of compatible elements. LSA has increasingly focused on the interaction of the slab-derived melts with peridotite and/or basalt in the mantle wedges (Gao et al., 2007; Kamber et al., 2002; Kelemen et al., 2003; Martin, 1999; Yogodzinski et al., 1995).

Archaean adakites are characterized by high Sr and low Y with high Sr/Y ratios of appropriately 50–100. They have strongly fractionated REE patterns (e.g., high La/Yb ratios, low Y, and Yb contents), and are almost

* Corresponding author.
E-mail address: Jamshidahmadian@yahoo.com (F. Sarjoughian).

http://dx.doi.org/10.1016/j.oregeorev.2015.07.017
0169-1368/

identical with typical adakites in composition. In addition, they are generally felsic (e.g., dacites and rhyolites) and have high Na_2O and low K_2O, so consequently quite low K_2O/Na_2O ratios (0.3–0.4) (Moyen, 2009).

Richards and Kerrich (2007) pointed out that a large portion of the calc-alkaline series does evolve into the adakitic field, and the evolution can be ascribed to processes like assimilation with fractional crystallization (AFC). Distinctive characteristics of arc rocks from this group are; (1) their association with non-adakitic rocks; (2) typically with low Sr/Y relative to the La/Yb values; (3) a generally potassic composition ($0.5 < K_2O/Na_2O < 1$); (4) somewhat lower MgO and $Mg^{\#}$, more similar to typical arc magmas than to adakites. This is because of decreasing the Y and HREE contents and increasing Sr/Y and La/Yb of arc magmas driving them into the adakitic field by fractionation of amphibole (Davidson et al., 2007) or garnet (Macpherson et al., 2006; Ulmer, 2007) from low or moderate Sr/Y and La/Yb andesite (Moyen, 2009).

A large group of rocks, also have been described as potassic adakites or continental adakites, with SiO_2 contents ranging from 60 to 75 wt.% and low Y and Yb values (Ding et al., 2007; Gao et al., 2007; Guo et al., 2006, 2007; Rapp et al., 2002; Wang et al., 2004a, Wang et al., 2007a, b; Xiao et al., 2007; Xu et al., 2004; Zhou et al., 2006). Continental adakites have high K_2O contents and high K/Na ratios (0.7–2.0) and Sr/Y ratios between 150 and 15 (Moyen, 2009). Models for the generation of continental adakites generally involve deep (>10–15 kbar) melting of the lower continental crust, either at the base of an orogenic wedge or as delaminated eclogites sinking in the mantle. In the latter case, it is proposed that interactions with the mantle can result in melts with higher MgO (Moyen, 2009). It is noteworthy that all the adakites attributed to lower crustal melting occur in arc settings (e.g., Atherton and Petford, 1993; Muir et al., 1995).

Several petrogenetic models have been proposed to account for the origin of adakitic rocks. These include: (1) partial melting of a young and hot subducted oceanic crust (e.g., Defant and Drummond, 1990; Kay et al., 1993; Martin et al., 2005; Stern and Kilian, 1996); (2) adakite–peridotite hybrid melt, melt derived from peridotite metasomatized by slab melt (e.g., Castillo, 2006); (3) partial melting of thickened lower crust (e.g., Chung et al., 2003; Hou et al., 2004; Wang et al., 2005; Zhang et al., 2001b); and (4) delaminated lower crust-derived adakitic rocks that have interacted with mantle peridotite (e.g., Chung et al., 2003; Gao et al., 2004; Huang et al., 2008; Kay and Kay, 1993; Wang et al., 2004a,b, Wang et al., 2006a,b; Xu et al., 2002).

Adakitic provinces have been identified in the NW of Iran (Jahangiri, 2007; Jamali and Mehrabi, 2015), in the central part of the Zagros orogen, around Anar (Omrani et al., 2008), in the eastern Iran, Bibi-Maryam (Delavari et al., 2014), and in the southeastern part of the Urumieh-Dokhtar Magmatic Arc (UDMA) that is considered to be one of the main Cu-bearing regions in the world and studied by many authors (e.g., Asadi et al., 2014; Ayati et al., 2013; Richards et al., 2012; Shafiei et al., 2009; Zarasvandi et al., 2007, 2013, 2015, and others). It is thought that ore-hosting porphyry systems of UDMA are generally restricted to Miocene intrusions (e.g., Shafiei et al., 2009) and shown that they have an adakitic affinity (Asadi et al., 2014; Richards et al., 2012; Shafiei et al., 2009; Zarasvandi et al., 2015). The ore-hosting porphyry systems of UDMA are Kuh Panj adakitic complex (e.g., Sarcheshmeh, Meiduk, Sungun, Darreh-Zerreshk, Dalli, Iju, Parkam, and Ali-Abad) and that the Kuh Panj adakitic porphyries are believed to have formed by partial melting of a thickened, juvenile lower crust source in a transitional, post-collisional to intracontinental setting which previously underwent underplating or storing of mantle-derived melts at the base of the crust (cf. Asadi et al., 2014).

It has also been recognized that adakites are often associated with Cu–Au mineralization, such as porphyry copper deposits and epithermal gold systems (e.g., Defant et al., 2002; Oyarzun et al., 2001; Qu et al., 2004; Thieblemont et al., 1997); Zhang et al. (2001a, 2002) proposed that giant porphyry copper deposits are related to adakitic, highly oxidized, and water-rich melts, although as noted earlier there are aspects of these magmatic systems that do not make this a universal feature.

In previous studies in the Kal-e-Kafi area, it has been postulated that a highly metasomatized mantle source with an increasing role of amphibole and garnet (0%–10%) in the genesis of the relatively younger granites (Ahmadian et al., 2009); in this paper, geochemical characteristics indicate that the multiphase Kal-e-Kafi intrusive complex has many adakitic petrogeochemical characteristics, but is poorly constrained geodynamically. A detailed account of the petrology and geochemistry of this prominent intrusive complex is presented that addresses its petrogenesis, of which the results help to better understand the complex magmatic evolution in an active continental margin setting during subduction and possibly collision. Furthermore, the relationship between these adakitic rocks and associated Cu, Mo, Au, and associated base-metal mineralization is discussed, providing valuable information on the geodynamic history and metallogenic potential of the area.

2. Geological setting

Iranian volcano-plutonic magmatic arc has been studied by Stöcklin (1968), Berberian and King (1981), Alavi (1994), Agard et al. (2005, 2011), Shahabpour (2007), and Omrani et al. (2008) and others. It is generally believed that the detachment of Central Iran from Arabia during Late Permian and its northwestward movement led to the formation of a new ocean (Neotethys) along the present main Zagros folded-thrust belt (Berberian and Berberian, 1981; Berberian and King, 1981). The Middle Triassic orogeny in Iran is interpreted as the result of subduction of the Neotethys oceanic crust underneath the Central Iran crustal block. The subduction of the Neo-Tethyan oceanic crust beneath the Iranian microcontinent sutured Iran to Arabia (e.g., Alavi, 1994; Berberian and King, 1981), and the subsequent continental convergence formed the Zagros Orogenic Belt. This orogenic belt is a part of the Alpine-Himalayan orogenic belt and consists of three NW-trending parallel zones: (1) UDMA; (2) Sanandaj-Sirjan Zone (SSZ); and (3) Zagros Fold-Thrust Belt (ZFTB) (Fig. 1). The UDMA extends as a 5–25 km wide and ~2000 km long NW-trending magmatic belt, aligned parallel to the suture of the collisional Zagros fold-thrust belt, which has been interpreted to be a subduction-related, Andean-type magmatic arc. Most of the studied magmatic rocks of UDMA are calc-alkaline magmas formed by the subduction of the Afro-Arabian plate under an active Iranian continental margin during Mesozoic up to the Eocene–Miocene time (e.g., Agard et al., 2011).

The Kal-e-Kafi igneous complex is located at 54°10′–54°20′N, 33°20′–33°30′E, and crops out over an area of 40 km^2. The Eocene intrusive rocks of Kal-e-Kafi, which are exposed in the Anarak area, are intruded into Upper Protrozoic and Paleozoic metamorphic rocks, lower Eocene volcanic rocks (including latite, dacite, and andesite tuffs) and partially covered by Quaternary sediment in the south and southwest part of the pluton. The Kal-e-Kafi intrusive complex is comprises; (1) gabbro, (2) monzonite–quartz monzonite, and (3) granite that was then intruded by diabase dikes (Fig. 1). The gabbro has a dark gray appearance, which is abundant in the eastern part of the intrusive complex, and light gray and pinkish monzonite–quartz monzonite with K-feldspar megacrysts is the most abundant lithology and includes abundant rounded and ellipsoid mafic microgranular enclaves. Granitic rocks in the western part of the pluton are light cream to white with smooth weathering surfaces (Fig. 2).

Another important aspect of the Kal-e-Kafi intrusive complex is that it is hosts various types of Cu, Au, and Mo mineralization. Thus far, 16 bore-holes have defined an ore body, with a reserve estimation of 245 Mt, with an average grade of 0.26% Cu and 0.026% Mo (Yakovenko et al., 1981). The area is cut by three major fault systems with N–S, E–W, and NE–SW trends, which were the main conduits for the mineralizing hydrothermal fluid. Stockwork-style mineralization (Cu and Mo) is located at the intersection of N–S and E–W faults, whereas polymetallic (Pb, Zn, W, Mo and Au) quartz-carbonate veins

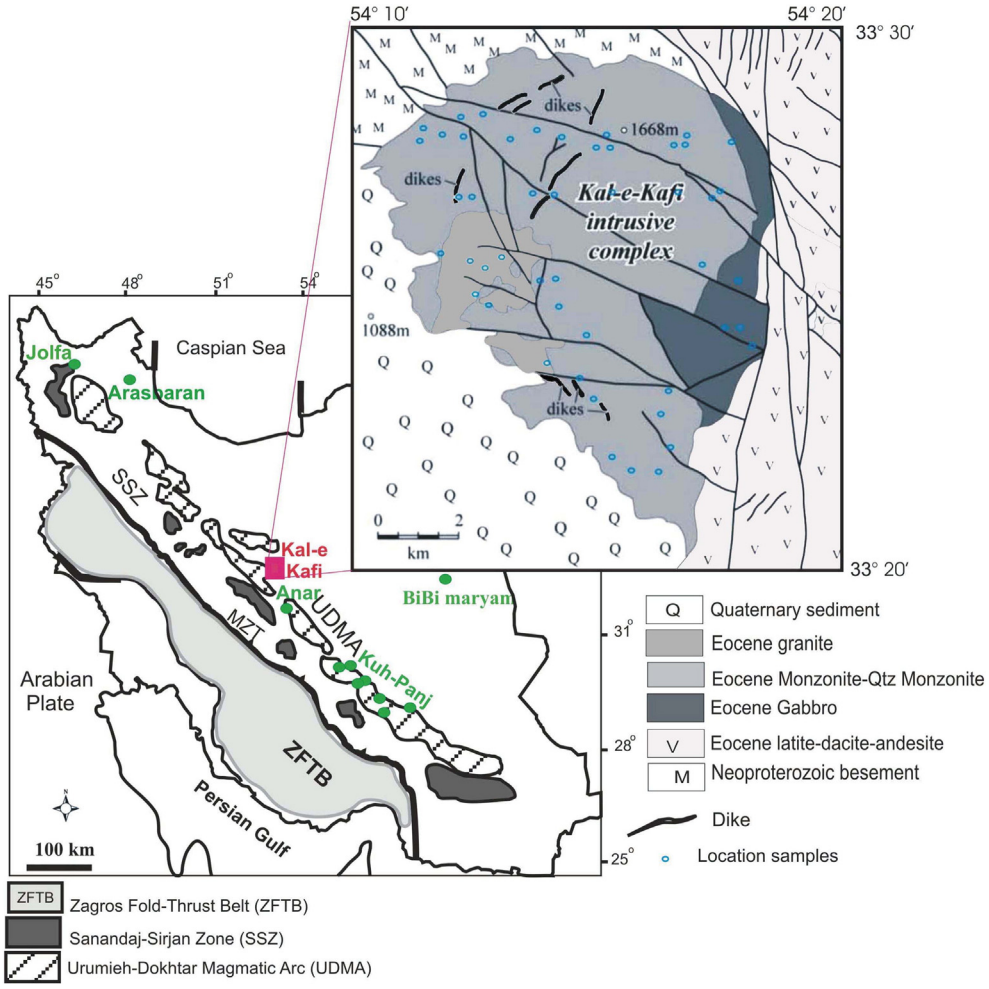

Fig. 1. Geological map of the Kal-e-Kafi intrusive complex in Central Iran, modified from Ahmadian et al. (2009). The circles are other reported adakite rocks in Iran.

are present in N–S faults. The main minerals defining the stockwork system are molybdenite, chalcopyrite, and pyrite as well as a second stage assemblage of magnetite, hematite, and bornite, galena, sphalerite, and electrum. Cu (Mo–Au) mineralization corresponds mainly to porphyry granite and quartz monzonite. The alteration zones in these rocks can be divided into four types which are represented by potassic, phyllic, argillic, and silicic (Fig. 3).

2.1. Analytical methods

Zircons were extracted using standard density and magnetic separation techniques from the two samples dated (see Table 1). Then zircon grains were handpicked under a binocular stereomicroscope and mounted on double sided adhesive tape, and set in Epirez™ resin. The mounted zircons were ground and polished to effectively cut them in half and then gold coated. Cathodoluminescence (CL) images were obtained to identify the internal structure of the zircons. U–Th–Pb analyses were performed using a SHRIMP II ion microprobe at Curtin University in Australia following techniques described by Williams (1998) utilizing five-cycle runs through the mass stations. The age calculations and plotting of concordia diagrams were made using Isoplot (ver. 3.23) (Ludwig, 2003). U–Pb dating was performed on 25 zircon grains separated from samples 154M and 101H obtain the formation age of the Kale-Kafi complex (Table 1).

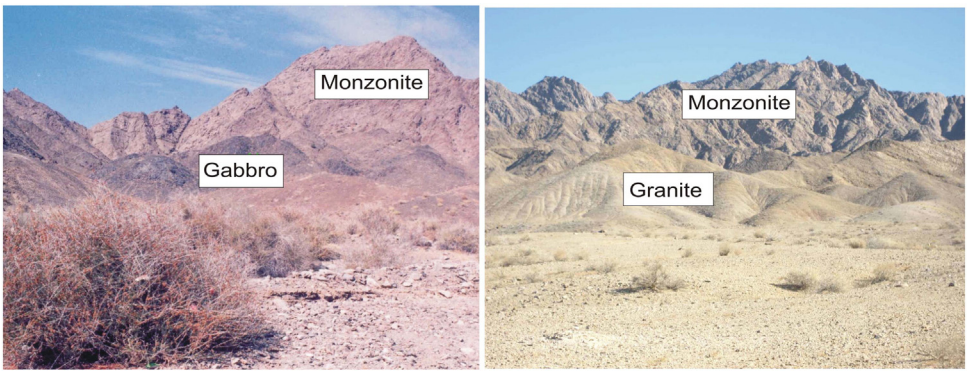

Fig. 2. Overview of the Kal-e-Kafi intrusive complex showing field relations of monzonite-gabbro and monzonite-granite.

Fig. 3. Vein-veinlet potassic alteration in quartz monzonite.

In the Kal-e-Kafi intrusive complex, 48 samples were collected (Fig. 1) for elemental and isotopic analysis (Table 2). The major elements were analyzed by X-ray fluorescence spectrometry (XRF) using fused glass disk at the Naruto University. XRF is Rigaku RIX 2000 with Rh end window tube. The samples were analyzed for major with a XRF wave length dispersive spectrometer (Rigaku RIX 2000). Glass beads, from finely grounded samples, were prepared with a sample to flux ($Li_2B_4O_7$) ratio of 1:10 and analyzed for major elements using the fundamental parameter method and analytical errors are usually less than 1% (see Murata, 1993).

Trace elements of selected samples, including the REE, were analyzed using a Perkin-Elmer ELAN 6100 ICP-MS at the Actlabs Ltd., Canada. Analytical precision for most elements is generally better than 3%. Some samples were analyzed by fusion inductively coupled plasma-mass spectroscopy (ICP-MS) and Emission Spectroscopy (ICP-ES) at Cardiff University, England. Instrumental precision for major elements by ICP-MS and ICP-ES methods are 1 to 3% and for trace elements 3 to 10%. Instrumental precision on low-abundance high field strength elements (HFSE, Ta, Hf, etc.) and REE is 2 to 12%, depending on the element and the sample. Trace elements of the other samples (marked by asterisk) were analyzed at the RWTH Aachen University by ICP-ES. The analytical precision for REE and Y is better than 4% and 5–10% for other trace elements. Strontium and Nd isotopes were analyzed by Marcel Regelous at Royal Holloway University London with unleached powder and calibrated against standards NBS987 (Sr mean, 0.710247; SD, 0.000009) and Aldrich (Nd mean, 0.511403; SD, 0.000008).

3. Petrography

The Kal-e-Kafi intrusive complex ranges in composition from olivine gabbro to monzonite–quartz monzonite to granite (Lemaitre et al., 1989; Fig. 4). The gabbro is coarse grained and displays an intercumulus texture composed of olivine, clinopyroxene, and plagioclase, with small amounts of amphibole, phlogopite, apatite, and magnetite. Olivine is subhedral to euhedral and some olivines are mantled by pyroxene or amphibole. Clinopyroxene is euhedral to subhedral and shows oscillatory normal zoning. Plagioclase occurs as subhedral to euhedral crystals and commonly displays polysynthetic twinning.

Monzonite and quartz monzonite rocks consist of the same minerals, but in different proportions across the intrusion. They show a granular medium-grained texture and comprise mainly of clinopyroxene, amphibole, plagioclase, phlogopite, and hornblende and rarely crystals of K-feldspar and accessory minerals, including titanite, apatite, zircon, and opaque minerals. Monzonite is transitional into quartz monzonite with a decrease of mafic minerals and increase of quartz. Clinopyroxene forms mainly subhedral to anhedral crystals and is locally present. Plagioclase occurs as euhedral to subhedral crystals and commonly shows concentric normal zoning and/or polysynthetic twinning. Amphiboles typically show a euhedral prismatic habit and are commonly twinned. Micas are dominantly phlogopite and display euhedral to subhedral habit. Quartz and K-feldspars are typically anhedral and occur as interstitial phases and (or) as large megacrysts.

Granitic rocks comprise amphibole, biotite, plagioclase, quartz, and K-feldspar with medium grained, granular, micrographic, granophyric, perthitic, and poikilitic textures. They contain less mafic minerals and more K-feldspar and quartz compared with other rock types. The plagioclase crystals occur as euhedral to subhedral crystals with normal and oscillatory zoning and commonly show polysynthetic twinning. Some plagioclases are mantled by orthoclase forming an antirapakivi texture (Fig. 5a). The K-feldspars are subhedral to anhedral, and in some samples show Carlsbad twinning and perthitic texture. Quartz occurs as anhedral to subhedral crystals or as a late interstitial phase, but locally forms micrographic to granophyric intergrowth (Fig. 5b); Shannon et al. (1982) and others believe that the micrographic and granophyric textures and porphyritic nature of granitic rocks associated with porphyry deposits are the result of pressure-quench crystallization related to the rapid escape of exsolving ore fluids. Mafic constituents including biotite and hornblende, occur as anhedral grains of which biotite is more abundant than amphibole. Zircon, apatite, and Fe–Ti-oxides are commonly present as fine inclusions in other minerals.

Monzonite and quartz monzonite dikes have porphyritic and trachytic textures characterized by abundant euhedral to subhedral phenocrysts of clinopyroxene and plagioclase, with less common biotite and hornblende. The same minerals, accompanied by anhedral quartz and K-feldspar, are present in the groundmass. Clinopyroxenes shows spongy texture and are characterized by oscillatory zoning. Plagioclase occurs as tabular grains, typically characterized by lamellar twinning and/or oscillatory zoning. Green hornblende and biotite are common mafic minerals with variable sizes. Alkaline feldspar mainly occurs as interstitial crystals amongst lath-shaped microlites. The accessory minerals mainly include magnetite, titanite, and apatite.

Early hydrothermal alteration was dominantly potassic and phyllic, that was followed by later argillic alteration, which was accompanied by veins with quartz. Potassic alteration is characterized by K-feldspar, irregularly shaped crystals of biotite, quartz, and locally sericite. In this zone, plagioclase is usually transformed into K-feldspar, while biotite was converted to secondary and/or recrystallized biotite (Fig. 6a). The phyllic alteration is widely observed at the surface, as well as selvages associated with veins and veinlets. Quartz, sericite, chlorite, and minor calcite constitute the phyllic alteration assemblage associated with pyrite and chalcopyrite veinlets (Fig. 6b) in deep parts of this zone. Cu-carbonates and Fe-oxides were formed in surficial supergene zones. The phyllic alteration grades gradually into the argillic type with increasing the amounts of clay minerals. The argillic alteration is composed of clay minerals that replace primary aluminosilicate phases, such as K-feldspar and plagioclase. X-ray diffraction (XRD) analysis indicates that kaolinite is the dominant phyllosilicate phase and is generally accompanied by dickite, sericite, quartz, hematite, limonite, and goethite. Silicification was synchronous with phyllic alteration and variably affected much of the stock and most dikes.

4. Zircon U–Pb geochronology

The zircon grains are mostly euhedral to subhedral and prismatic in shape and mostly stubby to elongated. Cathodoluminesence (CL) images mostly show oscillatory or growth zoning, consistent with an igneous origin with growth by magmatic processes (Hoskin and Schaltegger, 2003). CL images of some grains attest to the presence of pre-magmatic inherited zircon domains that may represent part of the source material of the magma, which haven't been examined. All samples show variable Th and U concentrations. Zircons from granite sample 152 M have 48–921 ppm Th, 72–786 ppm U, and Th/U ratios of 0.32–1.33, while the 101H zircons have 79–685 ppm Th, 127–650 ppm U, and Th/U ratios of 0.50–1.05; the results of zircon U–Pb analyses are listed in Table 1. For the Kal-e-Kafi intrusive complex, twelve analyzed zircons from quartz monzonite sample 152 M yielded a

Table 1
U–Th–Pb data for the Kal-e-Kafi complex.

Sample 152		152A-1	152A-2	152A-3	152A-4	152A-5	152A-6	152A-7	152A-8	152A-9	152A-10	152A-11	152A-12.1
Pb	ppm	8	4	1	3	2	1	66	67	1	33	1	1
U	ppm	786	377	91	327	230	153	72	518	102	449	124	117
Th	ppm	921	391	86	323	204	128	48	691	67	143	141	80
Th/U		1.17	1.04	0.94	0.99	0.89	0.84	0.67	1.33	0.66	0.32	1.14	0.69
$^{204}Pb/^{206}Pb$		0.00022	0.00097	0.00303	0.00063	0.00058	−0.00008	0.00001	0.00065	0.00061	0.00006	−0.00076	0.00040
$^{207}Pb/^{206}Pb$		0.05120	0.04263	0.06688	0.05200	0.05168	0.05775	0.26749	0.73949	0.04395	0.05452	0.05443	0.05808
+/−		0.00115	0.00686	0.02424	0.00660	0.00747	0.00286	0.00518	0.01076	0.02039	0.00084	0.00314	0.01686
$^{208}Pb/^{206}Pb$		0.3686	0.3265	0.3240	0.3207	0.2892	0.2929	26.1943	21.0544	0.2203	0.0977	0.3853	0.2588
+/−		0.0049	0.0169	0.0570	0.0163	0.0183	0.0106	0.2871	0.2281	0.0476	0.0018	0.0134	0.0396
$^{206}Pb/^{238}U$		0.0083	0.0082	0.0084	0.0082	0.0082	0.0082	0.0383	0.0065	0.0081	0.0732	0.0082	0.0083
+/−		0.0001	0.0001	0.0003	0.0001	0.0001	0.0002	0.0006	0.0001	0.0002	0.0007	0.0002	0.0002
$^{207}Pb/^{235}U$		0.06	0.05	0.08	0.06	0.06	0.07	1.41	0.67	0.05	0.55	0.06	0.07
+/−		0.00	0.01	0.03	0.01	0.01	0.00	0.04	0.01	0.02	0.01	0.00	0.02
$^{208}Pb/^{232}Th$		0.0026	0.0026	0.0029	0.0026	0.0027	0.0029	1.5003	0.1029	0.0027	0.0225	0.0028	0.0031
+/−		0.0000	0.0001	0.0005	0.0001	0.0002	0.0001	0.0290	0.0018	0.0006	0.0005	0.0001	0.0005
$^{207}Pb/^{235}U$	Age	58	48	75	58	58	64	895	518	48	445	60	65
$^{207}Pb/^{206}Pb$	Age	250	0	834	285	271	520	3291	4809	0	393	389	533
$^{208}Pb/^{232}Th$	Age	52	52	58	53	54	58	18,522	1980	54	450	56	63
$^{206}Pb/^{238}U$	Age	53	53	54	52	53	53	243	42	52	455	52	53

Sample 101		KA101-1.1	KA101-2.1	KA101-3.1	KA101-4.1	KA101-5.1	KA101-6.1	KA101-7.1	KA101-8.1	KA101-9.1	KA101-10.1	KA101-11.1	KA101-12.1
Pb	ppm	2	2	3	3	1	4	2	2	3	2	6	2
U	ppm	192	225	355	353	127	470	222	185	374	201	650	186
Th	ppm	110	130	209	244	79	374	164	133	187	122	685	115
Th/U		0.57	0.58	0.59	0.69	0.62	0.80	0.74	0.72	0.50	0.61	1.05	0.62
$^{204}Pb/^{206}Pb$		0.00124	0.00073	−0.00013	−0.00044	−0.00057	−0.00024	0.00165	0.00132	0.00018	0.00052	0.00022	0.00108
$^{207}Pb/^{206}Pb$		0.02901	0.04094	0.04859	0.04420	0.05006	0.04717	0.02861	0.03277	0.05006	0.03963	0.04553	0.03217
+/−		0.01308	0.01462	0.00167	0.00158	0.00329	0.00147	0.01441	0.01468	0.01029	0.01797	0.00563	0.01713
$^{208}Pb/^{206}Pb$		0.1537	0.1787	0.1897	0.2430	0.2216	0.2483	0.1745	0.1908	0.1722	0.1791	0.3149	0.1449
+/−		0.0307	0.0341	0.0058	0.0071	0.0111	0.0059	0.0338	0.0346	0.0240	0.0418	0.0140	0.0398
$^{206}Pb/^{238}U$		0.0079	0.0077	0.0079	0.0080	0.0076	0.0078	0.0077	0.0079	0.0085	0.0078	0.0077	0.0081
+/−		0.0002	0.0002	0.0002	0.0002	0.0002	0.0001	0.0002	0.0002	0.0002	0.0002	0.0002	0.0002
$^{207}Pb/^{235}U$		0.03	0.04	0.05	0.05	0.05	0.05	0.03	0.04	0.06	0.04	0.05	0.04
+/−		0.01	0.02	0.00	0.00	0.00	0.00	0.02	0.02	0.01	0.02	0.01	0.02
$^{208}Pb/^{232}Th$		0.0021	0.0024	0.0026	0.0028	0.0027	0.0024	0.0018	0.0021	0.0029	0.0023	0.0023	0.0019
+/−		0.0004	0.0005	0.0001	0.0001	0.0001	0.0001	0.0004	0.0004	0.0004	0.0005	0.0001	0.0005
$^{207}Pb/^{235}U$	Age	31	43	52	49	52	50	30	36	58	42	48	36
$^{207}Pb/^{206}Pb$	Age	0	0	128	0	198	62	0	0	198	0	0	0
$^{208}Pb/^{232}Th$	Age	43	48	52	57	55	49	37	42	59	46	47	38
$^{206}Pb/^{238}U$	Age	51	49	51	52	49	50	49	51	55	50	50	52

Table 2
The result of major oxides (wt.%), trace element (ppm), and isotopic data in the Kal-e-Kafi intrusive complex.

Sample	10G	109G	112G	48G	78G	80G	81G	104 M	39 M	50 M	152 M	162 M
SiO_2	66.40	69.68	70.51	74.47	67.50	71.12	70.61	66.97	66.33	67.26	66.26	66.98
TiO2	0.29	0.17	0.12	0.11	0.20	0.19	0.19	0.26	0.32	0.33	0.36	0.30
Al_2O_3	17.56	16.90	17.94	15.07	19.85	16.08	15.96	17.39	16.31	16.00	16.35	15.90
Fe_2O_3	2.49	1.18	0.53	0.65	1.51	1.46	1.16	2.14	2.61	2.64	1.94	2.43
MnO	0.04	0.01	0.00	0.01	0.01	0.02	0.02	0.03	0.05	0.06	0.06	0.05
MgO	0.65	0.43	0.33	0.02	0.36	0.36	0.30	0.76	0.89	1.02	1.37	0.86
CaO	2.40	1.87	1.50	0.51	1.96	2.11	2.08	2.39	2.20	2.61	3.29	2.43
Na_2O	4.70	4.56	3.60	4.13	4.98	5.20	5.16	5.30	5.44	5.31	5.59	5.21
K_2O	4.08	5.02	5.33	5.06	3.07	3.40	3.37	4.10	4.96	4.58	4.31	4.87
P_2O_5	0.17	0.04	0.05	0.03	0.04	0.04	0.04	0.09	0.13	0.13	0.17	0.13
LOI	1.19	0.04	0.87	0.62	0.85	0.03	1.11	0.89	0.76	0.05	0.29	0.84
Total	99.97	99.90	100.78	100.68	100.33	100.01	100.00	100.32	100.00	99.99	99.99	100.00
Ba	752	418	541	223	808	789	1110	678	772	715	883	822
Rb	119	129	102	139	89	84	84	109	137	144	134	128
Sr	1433	897	926	400	1053	964	986	1250	1300	1360	1320	1200
Cs	[a]	[a]	[a]	[a]	[a]	1.70	1.80	[a]	3.60	8.30	1.80	2.00
Ga	22.50	20.80	22.20	22.80	21.90	20.00	20.00	22.00	24.00	24.00	21.00	20.00
Ta	6.50	5.00	6.50	9.10	6.60	0.52	0.48	10.20	0.88	0.82	0.87	0.86
Nb	11.80	12.80	10.80	16.00	10.80	9.00	8.40	13.60	12.50	12.50	12.80	12.10
Hf	5.60	4.50	4.40	7.50	6.30	3.40	3.30	5.80	5.40	5.40	5.50	5.20
Zr	204.10	120.30	81.50	102.40	142.00	123.00	123.00	166.30	211.00	205.00	204.00	199.00
Y	[a]	[a]	[a]	[a]	[a]	9.00	8.80	[a]	14.60	13.70	14.80	14.00
Th	[a]	[a]	23.30	33.70	[a]	6.02	5.29	[a]	16.20	20.00	13.30	10.30
U	2.20	2.10	[a]	2.00	[a]	1.80	1.87	2.10	3.27	3.24	3.77	3.10
Cr	44.60	[a]	[a]	[a]	[a]	[a]	10.00	25.20	28.00	24.00	29.00	26.00
Ni	26.90	12.50	11.80	15.00	10.20	[a]	[a]	18.10	53.00	20.00	[a]	23.00
Co	89.30	79.70	79.90	137.30	101.60	2.00	3.00	111.20	5.00	5.00	4.00	5.00
V	46.70	17.10	13.00	[a]	[a]	14.00	14.00	28.70	64.00	57.00	35.00	41.00
La	30.20	22.00	14.30	32.60	15.00	19.90	17.90	27.80	37.60	36.10	35.70	35.30
Ce	55.00	[a]	[a]	[a]	[a]	35.50	33.40	50.00	67.50	62.50	62.70	61.80
Pr	10.30	4.50	7.20	3.50	12.50	3.63	3.33	7.40	6.88	6.32	6.61	6.32
Nd	27.10	10.90	10.40	3.60	10.60	12.20	11.10	20.60	24.90	23.10	24.50	23.10
Sm	[a]	[a]	[a]	[a]	[a]	2.17	2.13	[a]	4.38	3.97	4.42	4.08
Eu	[a]	[a]	[a]	[a]	[a]	0.64	0.62	[a]	1.14	1.05	1.14	1.05
Gd	[a]	[a]	[a]	[a]	[a]	1.66	1.54	[a]	3.29	2.95	3.34	2.99
Tb	[a]	[a]	[a]	[a]	[a]	0.27	0.26	[a]	0.50	0.45	0.50	0.47
Dy	[a]	[a]	[a]	[a]	[a]	1.43	1.39	[a]	2.45	2.25	2.52	2.29
Ho	[a]	[a]	[a]	[a]	[a]	0.28	0.28	[a]	0.46	0.42	0.47	0.44
Er	[a]	[a]	[a]	[a]	[a]	0.85	0.86	[a]	1.39	1.30	1.39	1.36
Tm	[a]	[a]	[a]	[a]	[a]	0.14	0.14	[a]	0.22	0.21	0.22	0.22
Yb	[a]	[a]	[a]	[a]	[a]	0.95	0.95	[a]	1.48	1.36	1.41	1.34
Lu	[a]	[a]	[a]	[a]	[a]	0.15	0.15	[a]	0.22	0.21	0.22	0.21
$mg^{\#}$	0.22	0.29	0.41	0.03	0.21	0.22	0.22	0.28	0.27	0.30	0.44	0.28
Sr/Y	[a]	[a]	[a]	[a]	[a]	107.11	112.05	[a]	89.04	99.27	89.19	85.71
La/Yb	[a]	[a]	[a]	[a]	[a]	20.95	18.84	[a]	25.41	26.54	25.32	26.34
$(^{87}Sr/^{86}Sr)_i$	[a]	[a]	[a]	[a]	[a]	[a]	[a]	[a]	[a]	[a]	0.7047	[a]
$(^{143}Nd/^{Nd}144)_i$	[a]	[a]	[a]	[a]	[a]	[a]	[a]	[a]	[a]	[a]	0.5126	[a]
εNd	[a]	[a]	[a]	[a]	[a]	[a]	[a]	[a]	[a]	[a]	0.21	[a]

Sample	77 M	161 M	18 M	45 M	111 M	75 M	190D	166D	2D	24D	52D
SiO_2	58.16	62.14	57.78	59.49	58.61	62.44	52.72	61.11	57.00	61.33	60.13
TiO2	0.59	0.26	0.83	0.52	0.66	0.32	0.93	0.56	0.61	0.54	0.50
Al_2O_3	16.28	20.34	16.13	17.17	16.56	16.34	14.67	15.45	12.86	15.58	18.76
Fe_2O_3	5.33	1.07	6.85	4.63	5.54	4.04	8.32	5.05	5.09	4.87	4.20
MnO	0.09	0.04	0.13	0.08	0.09	0.06	0.14	0.10	0.07	0.10	0.07
MgO	3.26	0.81	3.23	2.05	2.35	2.04	5.87	3.12	6.74	2.96	2.11
CaO	4.76	5.33	6.34	4.23	4.21	3.24	7.95	4.44	6.77	4.19	4.04
Na_2O	5.64	7.58	4.23	5.70	5.58	5.46	3.87	4.29	5.50	4.40	5.18
K_2O	4.57	0.83	3.29	4.95	5.01	4.95	3.79	4.37	1.56	4.56	4.64
P_2O_5	0.53	0.07	0.40	0.34	0.38	0.28	0.67	0.37	0.66	0.37	0.35
LOI	0.79	1.53	0.78	0.77	1.29	0.83	1.05	1.15	3.13	1.09	0.84
Total	100.00	100.00	99.99	99.93	100.28	100.00	99.98	100.01	99.99	99.99	100.82
Ba	733	160	489	659	632	594	649	609	146	610	652
Rb	87	23	73	103	112	111	55	95	45	117	125
Sr	1880	1090	1130	1892	1832	1530	1640	1140	772	1230	1659
Cs	2.70	0.50	1.50	[a]	[a]	2.90	2.10	5.30	2.00	4.60	2.10
Ga	21.00	31.00	25.00	23.50	22.00	25.00	20.00	19.00	16.00	20.00	18.20
Ta	0.35	0.78	0.69	5.80	5.10	0.39	0.30	0.74	0.56	0.66	9.30
Nb	6.80	14.40	11.70	10.30	13.10	7.30	6.30	9.70	9.10	9.70	10.10
Hf	3.30	6.00	4.70	6.30	5.40	6.30	3.10	4.70	4.00	4.70	3.20
Zr	133.00	181.00	184.00	221.00	226.10	288.00	114.00	181.00	142.00	178.00	182.30
Y	14.70	9.80	23.30	[a]	[a]	10.80	20.40	15.80	16.10	16.00	[a]
Th	5.05	41.60	8.02	[a]	[a]	7.87	5.41	11.60	8.71	11.60	[a]
U	1.29	11.70	2.31	2.20	2.30	2.48	1.47	3.76	3.47	3.66	2.40
Cr	68.00	14.00	38.00	74.90	[a]	39.00	98.00	82.00	335.00	82.00	161.20

Table 2 (*continued*)

Sample	77 M	161 M	18 M	45 M	111 M	75 M	190D	166D	2D	24D	52D
Ni	54.00	39.00	20.00	44.20	44.30	32.00	65.00	35.00	122.00	36.00	77.80
Co	14.00	10.00	17.00	73.10	50.10	8.00	28.00	13.00	13.00	9.00	66.90
V	98.00	29.00	165.00	88.70	18.90	93.00	201.00	82.00	107.00	93.00	148.50
La	32.70	25.40	34.80	31.40	33.00	29.20	35.20	27.80	20.40	29.60	32.60
Ce	64.50	45.80	69.50	61.10	66.50	50.90	70.50	55.40	44.40	57.20	71.40
Pr	7.38	4.25	7.89	5.90	9.10	5.22	8.40	6.23	5.08	6.44	4.60
Nd	29.60	14.70	31.20	19.10	28.70	18.80	34.10	24.80	19.60	24.30	15.40
Sm	5.63	2.38	6.04	[a]	[a]	3.12	7.27	4.73	4.25	4.84	[a]
Eu	1.64	0.62	1.71	[a]	[a]	0.98	2.11	1.27	1.25	1.30	[a]
Gd	4.42	1.68	5.14	[a]	[a]	2.50	5.73	3.93	3.51	3.80	[a]
Tb	0.57	0.27	0.77	[a]	[a]	0.33	0.80	0.56	0.57	0.56	[a]
Dy	2.72	1.42	4.08	[a]	[a]	1.68	3.80	2.94	2.93	2.81	[a]
Ho	0.48	0.28	0.78	[a]	[a]	0.32	0.69	0.54	0.56	0.54	[a]
Er	1.36	0.92	2.33	[a]	[a]	0.97	1.91	1.59	1.62	1.55	[a]
Tm	0.19	0.16	0.35	[a]	[a]	0.15	0.27	0.25	0.24	0.24	[a]
Yb	1.21	1.13	2.26	[a]	[a]	1.05	1.71	1.61	1.51	1.59	[a]
Lu	0.18	0.20	0.33	[a]	[a]	0.17	0.24	0.24	0.21	0.23	[a]
mg#	0.40	0.46	0.34	0.33	0.32	0.36	0.44	0.41	0.60	0.40	0.36
Sr/Y	127.89	111.22	48.50	[a]	[a]	141.67	80.39	72.15	47.95	76.88	[a]
La/Yb	27.02	22.48	15.40	[a]	[a]	27.81	20.58	17.27	13.51	18.62	[a]
$(^{87}Sr/^{86}Sr)_i$	0.7042	[a]	[a]	[a]	[a]	0.7043	0.7042	[a]	[a]	0.7045	[a]
$(^{143}Nd/^{Nd}144)_i$	0.5127	[a]	[a]	[a]	[a]	0.5127	0.5127	[a]	[a]	0.5126	[a]
εNd	2.15	[a]	[a]	[a]	[a]	1.72	1.75	[a]	[a]	0.51	[a]

Sample	6D	60D	62D	66D	76D	96D	124D	112D	113D	101H	135H	140H
SiO_2	60.62	56.08	57.43	54.77	68.04	54.82	58.47	61.14	64.48	69.60	69.52	74.39
TiO2	0.41	0.69	0.63	0.92	0.19	0.64	0.73	0.18	0.32	0.24	0.22	0.09
Al_2O_3	14.79	15.57	15.61	15.18	19.23	18.90	16.94	19.62	16.88	15.70	16.13	13.56
Fe_2O_3	3.56	6.33	5.81	7.41	1.12	6.03	5.45	1.72	1.99	2.06	1.89	0.44
MnO	0.07	0.10	0.10	0.13	0.02	0.10	0.12	0.02	0.03	0.04	0.04	0.01
MgO	4.02	4.31	3.90	4.49	0.24	3.86	1.94	0.55	0.82	0.16	0.02	0.02
CaO	4.31	5.61	5.12	6.78	1.72	5.40	5.61	2.24	1.95	2.38	2.13	0.80
Na_2O	5.09	4.90	5.02	4.22	6.08	4.74	5.19	7.47	4.95	5.20	5.31	3.72
K_2O	4.56	4.60	4.61	4.49	5.96	4.38	3.63	4.79	7.08	4.49	4.30	5.83
P_2O_5	0.26	0.55	0.48	0.55	0.07	0.58	0.28	0.11	0.16	0.13	0.05	0.11
LOI	2.32	1.26	1.29	1.05	0.00	1.07	1.64	0.67	1.32	0.69	0.38	0.75
Total	100.01	100.00	100.00	99.99	102.67	100.52	100.00	98.51	99.98	100.69	99.99	99.72
Ba	625	610	634	640	662	668	642	770	583	709	697	215
Rb	158	101	96	110	124	102	90	83	113	110	110	160
Sr	742	1630	1530	1290	1820	1634	1450	3063	1334	1077	1097	393
Cs	6.30	5.70	3.00	6.20	2.90	[a]	2.50	4.02	2.02	[a]	[a]	[a]
Ga	20.00	21.00	20.00	22.00	24.00	22.40	24.00	[a]	[a]	23.40	19.50	24.40
Ta	0.73	0.49	0.47	0.70	0.41	10.20	0.61	0.36	1.10	8.10	5.30	9.70
Nb	10.90	8.80	8.40	11.20	6.40	9.90	11.30	4.49	10.99	11.60	10.60	9.20
Hf	5.40	4.50	4.20	5.00	4.90	6.00	4.60	1.68	5.91	6.60	5.60	7.40
Zr	196.00	172.00	160.00	186.00	186.00	179.60	180.00	67.40	237.80	157.60	140.00	111.00
Y	16.00	17.30	15.90	19.30	5.40	[a]	23.80	5.90	9.40	[a]	[a]	[a]
Th	15.30	9.21	8.50	12.50	8.16	[a]	9.02	9.65	14.65	[a]	[a]	34.20
U	5.88	3.20	2.86	3.53	2.98	2.20	2.25	2.20	4.28	2.00	2.00	[a]
Cr	233.00	99.00	102.00	62.00	10.00	90.00	15.00	40.80	37.40	[a]	19.20	[a]
Ni	88.00	61.00	56.00	42.00	[a]	51.50	[a]	26.10	21.10	17.90	[a]	13.60
Co	10.00	19.00	18.00	19.00	4.00	125.50	8.00	2.80	5.70	161.90	56.60	[a]
V	71.00	131.00	123.00	168.00	21.00	127.40	109.00	38.80	47.40	[a]	21.00	[a]
La	37.00	33.90	29.70	34.70	15.90	31.40	35.30	17.21	17.86	24.80	26.10	15.60
Ce	73.20	65.90	60.20	68.70	26.90	64.30	70.00	29.09	34.54	48.20	45.80	[a]
Pr	8.25	7.70	6.88	7.97	2.71	8.60	7.79	3.12	3.63	3.80	3.80	[a]
Nd	31.00	29.80	26.60	30.90	9.59	26.50	29.90	11.03	12.71	14.40	16.00	[a]
Sm	5.95	6.16	5.54	6.47	1.75	[a]	6.16	2.03	2.25	[a]	[a]	[a]
Eu	1.50	1.75	1.56	1.81	0.69	[a]	1.74	1.24	0.98	[a]	[a]	[a]
Gd	4.41	4.66	4.23	5.18	1.26	[a]	4.93	1.52	1.82	[a]	[a]	[a]
Tb	0.61	0.65	0.61	0.75	0.18	[a]	0.77	0.19	0.25	[a]	[a]	[a]
Dy	2.81	3.17	2.92	3.69	0.87	[a]	4.04	1.01	1.38	[a]	[a]	[a]
Ho	0.50	0.57	0.54	0.68	0.16	[a]	0.80	0.17	0.26	[a]	[a]	[a]
Er	1.51	1.64	1.49	1.91	0.49	[a]	2.26	0.53	0.86	[a]	[a]	[a]
Tm	0.22	0.24	0.21	0.28	0.08	[a]	0.35	0.08	0.15	[a]	[a]	[a]
Yb	1.47	1.49	1.39	1.78	0.56	[a]	2.22	0.53	1.04	[a]	[a]	[a]
Lu	0.22	0.22	0.21	0.26	0.09	[a]	0.33	0.08	0.17	[a]	[a]	[a]
mg#	0.56	0.43	0.43	0.40	0.19	0.42	0.28	0.26	0.31	0.08	0.01	0.05
Sr/Y	46.38	94.22	96.23	66.84	337.04	[a]	60.92	519.08	141.86	[a]	[a]	[a]
La/Yb	25.17	22.75	21.37	19.49	28.39	[a]	15.90	32.47	17.17	[a]	[a]	[a]
$(^{87}Sr/^{86}Sr)_i$	[a]	0.7042	[a]	[a]	[a]	[a]	[a]	[a]	[a]	[a]	[a]	[a]
$(^{143}Nd/^{Nd}144)_i$	[a]	0.5127	[a]	[a]	[a]	[a]	[a]	[a]	[a]	[a]	[a]	[a]
εNd	[a]	2.35	[a]	[a]	[a]	[a]	[a]	[a]	[a]	[a]	[a]	[a]

(*continued on next page*)

Table 2 (*continued*)

Sample	100H	105H	170H	174H	176H	178H	180H	118 M	113B	109	109B	190B
SiO_2	70.81	68.77	70.94	71.07	69.25	64.59	69.77	52.69	41.47	38.52	41.77	51.55
TiO2	0.23	0.32	0.24	0.19	0.24	0.22	0.21	0.92	2.69	1.86	1.49	0.98
Al_2O_3	16.27	15.95	17.24	14.49	15.48	14.28	14.91	16.9	12.92	14.94	17.83	15.42
Fe_2O_3	1.55	2.19	0.62	0.94	1.27	2.71	1.34	8.06	13.86	15.58	12.13	8.93
MnO	0.02	0.03	0.02	0.02	0.02	0.16	0.03	0.14	0.22	0.22	0.18	0.15
MgO	0.37	0.20	0.23	0.24	0.38	1.42	0.42	4.68	11.53	9.78	8.49	6.1
CaO	1.95	1.05	0.56	1.85	1.36	3.04	1.61	7.16	12.45	15.46	14.67	8.82
Na_2O	4.97	4.75	4.42	3.53	4.44	0.76	3.66	4.47	2.31	1.59	1.82	3.19
K_2O	4.70	5.26	2.43	5.95	5.59	6.75	5.97	4.04	1.14	0.22	0.32	3.79
P_2O_5	0.08	0.14	0.08	0.08	0.08	0.08	0.06	0.47	0.13	1.21	0.79	0.62
LOI	0.00	1.34	3.23	1.64	1.88	6.00	2.02	0.81	1.28	0.79	0.9	0.35
Total	100.95	100.00	100.01	100.00	99.99	100.01	100.00	100.34	100	100.17	100.39	99.9
Ba	728	830	265	757	899	715	689	601.9	305	191	208.8	709.1
Rb	126	186	76	167	179	202	185	84.5	10	9	9	57.8
Sr	1050	880	623	728	785	305	544	1565	777	1829	2483	1801
Cs	[a]	[a]	[a]	[a]	[a]	[a]	[a]	[a]	0.5	[a]	[a]	[a]
Ga	[a]	[a]	[a]	[a]	[a]	[a]	[a]	21.6	21	22.4	24.2	20.4
Ta	0.79	0.78	0.76	0.70	0.79	0.64	0.65	8.5	0.7	7.2	7	6.9
Nb	11.40	11.30	11.30	11.00	11.10	10.20	8.70	10	18.2	[a]	[a]	[a]
Hf	4.40	4.80	4.10	3.90	4.20	3.70	3.90	6.1	4.5	3.7	3.4	3.3
Zr	185.00	189.00	159.00	152.00	156.00	141.00	140.00	166.5	121	43.4	39.2	80.5
Y	13.20	13.00	12.30	8.00	10.50	7.90	10.50	19.2	58.3	29.1	23.2	18.7
Th	11.90	19.00	7.71	12.00	12.70	9.68	11.80	[a]	0.5	[a]	[a]	[a]
U	2.76	8.52	1.58	3.37	3.99	4.36	6.36	2.1	0.14	[a]	[a]	[a]
Cr	[a]	[a]	[a]	[a]	[a]	[a]	[a]	73.7	31	221.2	245.9	153.6
Ni	[a]	[a]	[a]	[a]	[a]	[a]	[a]	41.6	85	94	103.6	70.2
Co	[a]	[a]	[a]	[a]	[a]	[a]	[a]	89.8	51	105	97.2	115.6
V	[a]	[a]	[a]	[a]	[a]	[a]	[a]	178.7	353	505	379.8	216
La	30.70	33.40	19.40	17.40	18.70	23.00	22.40	28.7	18.1	35.9	29	33.9
Ce	57.40	57.50	36.50	29.80	39.70	40.00	41.00	67.8	57.1	83.3	67	73
Pr	5.84	5.99	5.83	2.96	4.32	3.93	4.10	5	8.94	6.7	4.8	8.3
Nd	20.80	21.70	22.90	10.80	15.60	13.70	14.60	13.5	45.8	22.6	20.7	28.6
Sm	3.55	3.86	4.17	1.94	2.83	2.21	2.54	[a]	12	[a]	[a]	[a]
Eu	0.94	1.00	0.92	0.55	0.72	0.54	0.63	[a]	3.5	[a]	[a]	[a]
Gd	2.69	2.95	3.26	1.49	2.18	1.53	1.95	[a]	12.1	[a]	[a]	[a]
Tb	0.39	0.43	0.45	0.24	0.34	0.25	0.30	[a]	1.95	[a]	[a]	[a]
Dy	2.06	2.20	2.17	1.22	1.70	1.21	1.61	[a]	10.6	[a]	[a]	[a]
Ho	0.39	0.41	0.40	0.25	0.33	0.24	0.32	[a]	1.96	[a]	[a]	[a]
Er	1.23	1.28	1.13	0.78	1.00	0.77	1.01	[a]	5.73	[a]	[a]	[a]
Tm	0.20	0.20	0.17	0.13	0.17	0.12	0.17	[a]	0.802	[a]	[a]	[a]
Yb	1.27	1.28	1.11	0.84	1.09	0.84	1.15	[a]	4.84	[a]	[a]	[a]
Lu	0.19	0.19	0.17	0.14	0.18	0.14	0.19	[a]	0.658	[a]	[a]	[a]
$mg^{\#}$	0.21	0.09	0.29	0.22	0.25	0.37	0.26	0.39	0.4804	0.41	0.44	0.43
Sr/Y	79.55	67.69	50.65	91.00	74.76	38.61	51.81	81.51	13.328	62.85	107.03	96.31
La/Yb	24.17	26.09	17.48	20.71	17.16	27.38	19.48	[a]	3.7397	[a]	[a]	[a]
$(^{87}Sr/^{86}Sr)_i$	[a]	[a]	[a]	[a]	[a]	[a]	[a]	[a]	[a]	[a]	[a]	[a]
$(^{143}Nd/^{Nd}144)_i$	[a]	[a]	[a]	[a]	[a]	[a]	[a]	[a]	[a]	[a]	[a]	[a]
εNd	[a]	[a]	[a]	[a]	[a]	[a]	[a]	[a]	[a]	[a]	[a]	[a]

[a] : Not determined.

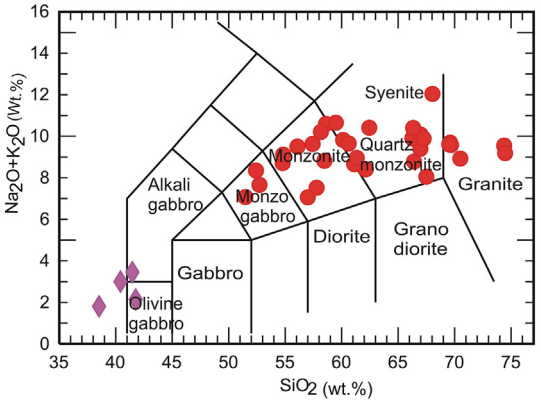

Fig. 4. Classification Kal-e-Kafi intrusive complex, using the Alkali vs. SiO_2 diagram (Lemaitre et al., 1989). Symbols: diamond: gabbroic rock, Circle: monzonite–quartz monzonite, monzodiorite–quartz monzodiorite, granite rocks.

concordia age of 52 ± 1 Ma with an MSWD of 0.25 (Fig. 7a), whereas twelve analyzed zircons from granite sample 101H resulted in a concordia age of 50.3 ± 1.1 Ma (n = 6) (Fig. 7b), which are considered to represent the age of emplacement of these intrusions.

5. Geochemical composition

The Kal-e-Kafi intrusive complex is mainly classified and subdivided into gabbro, monzonite-quartz monzonite, and granite. They (except for the gabbroic phase) have SiO_2 ranging from 52.72 to 74.47 wt.% and Al_2O_3 from 12.86 to 20.34 wt.%. Their Na_2O contents range from 3.53 to 7.58 wt.% and K_2O from 2.43 to 7.08 wt.% with low $Mg^{\#}$, Ni, and Cr contents (ave.: 44, 39, and 69 ppm, respectively). In addition, all samples exhibit high Sr (ave.: 1227 ppm), and low Y (ave.: 13 ppm), and Yb (ave.: 1.28 ppm) contents resulting in high Sr/Y (ave.: 108.4) and La/Yb (ave.: 22.2), jointly indicating that the studied intrusions can be classified having an adakitic affinity. Also, high Zr/Sm (ave.: 48.3) ratios are also comparable with modern adakites (Foley et al., 2002). Moreover, the adakitic affinity of the studied rocks becomes apparent in the Sr/Y vs. Y discrimination diagram (Defant and Drummond, 1990;

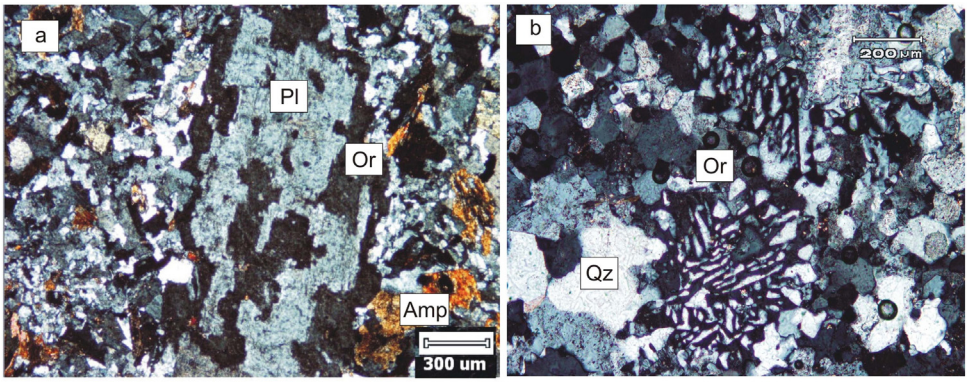

Fig. 5. Photomicrographs showing the mineralogy and textures of granitic rocks in the study area; (a) anti-rapakivi texture (XPL), (b) micrographic and granophyric intergrowth (XPL). Abbrevations: or: orthoclase, plg: plagioclase, Qz: quartz, and Am: amphibole (Whitney and Evans, 2010).

Fig. 8). Discriminating features of adakite magmas have been used to trace magma sources with the presence of garnet and rutile and the absence of plagioclase (Chung et al., 2003; Rapp and Watson, 1995; Rapp et al., 1991; Fu et al., 2012).

However, other typical features of adakites are high Na_2O contents (3.5–7.5 wt.%) and low K_2O/Na_2O ratio (<0.42), which clearly contrast with the K-rich compositions of the Kal-e-Kafi intrusive complex (ave.: K_2O/Na_2O: 1.11). These mentioned geochemical features are compatible with the shoshonitic series, based on the classification of Peccerillo and Taylor (1976), Pearce (1982), and Liegeois et al. (1998; not shown). Therefore, a suitable petrogenetic model for these granitoids must reconcile both adakitic and shoshonitic affinities of the studied intrusion. As Xiao and Clemens (2007) had suggested that a category of adakites that displays K-rich adakitic features should be defined; the features of the studied granitoids suggest that these rocks are similar to K-rich adakites.

In the NMORB-normalized multi-element spider diagram (Sun and McDonough, 1989; Fig. 9a), all samples are enriched in LILEs and depleted in HFSEs, with pronounced negative anomalies of Nb, P, and Ti and positive anomalies of Sr. These features are typical of the subduction-related magmas, namely in the calc-alkaline volcanic arcs of continental active margins (e.g., Pearce, 1983; Wilson, 1989). The chondrite-normalized REE patterns (Sun and McDonough, 1989) of the studied intrusion (Fig. 9b) are enriched in the LREEs relative to the HREEs with $(La/Yb)_N$ ranging from 16.6 to 26.7 and lack an Eu anomaly.

The gabbros have different major and trace elements compared to the other rock types and have relatively low SiO_2 (ave.: 42.2 wt.%), high $Mg^{\#}$ (ave.: 52), Cr (ave.: 145 ppm), and Ni (ave.: 79 ppm) contents. The high concentrations of these elements in the gabbroic rocks indicate that they could be cumulates (see Chappell, 1996). Feeley and Cosca (2003) also suggested that the enrichments in MgO, Ni, and Cr probably reflect concentration of these elements by olivine plus clinopyroxene accumulation. In addition, the NMORB-normalized and chondrite-normalized REE patterns show that gabbros and the other rock types are not similar to each other, as the former may show a signature of cumulus origin involving dominantly olivine, clinopyroxene, and hornblende accumulation (Himmelberg and Loney, 1995).

Strontium and Nd isotopic compositions were determined for six whole-rock samples. Considering ages of 50 Ma for the studied intrusion, the calculated initial $^{87}Sr/^{86}Sr$ ratios range between 0.704193 and 0.704688; the initial $^{143}Nd/^{144}Nd$ ratios vary from 0.512609 to 0.512706 and are relatively homogeneous. In the Nd–Sr isotope diagram (Fig. 10), all the studied granitoid samples plot in the center of the diagram, in the field of underplated thick lower crust-derived adakitic rocks, e.g., Separation Point Batholith of New Zealand (Muir et al., 1995), delaminated lower crust-derived adakitic rocks (Wang et al., 2006b). They also have much lower $\varepsilon Nd(t)$ than those of 400–179 Ma MORB (Mahoney et al., 1998; Tribuzio et al., 2004; Xu et al., 2003; Xu and Castillo, 2004) and Cenozoic adakites formed by slab melting (Aguillon-Robles et al., 2001; Kay et al., 1993; Wang et al., 2006b).

6. Discussion

6.1. Tectonic setting

The Kal-e-Kafi intrusive complex shows enrichment in LILE and LREE, relative to HREE and HFSE with negative anomalies in Ti, P, and Nb that display close similarities to those of the magmatic arc granites (Pearce et al., 1984). The high Ba/Zr (Ajaji et al., 1998) and Ba/Nb (Fitton et al., 1988) ratios are also indicative of subduction-related orogenic magmatism, because the high field strength elements (e.g., Zr, Nb, and Ti) are conservative and retained in the subducting slab, while the low field strength elements (e.g., Rb, Sr, K, Ba) are highly nonconservative and easily transported to the overlying zone of mantle melting

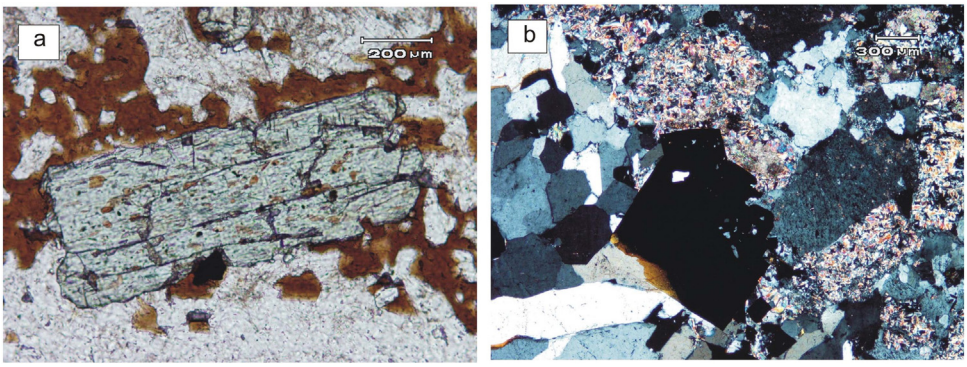

Fig. 6. Photomicrographs of (a) weakly potassic alteration evident as biotitization in microsyenite (PPL); (b) pervasive phyllic alteration in granitic rocks with opaque (CPL).

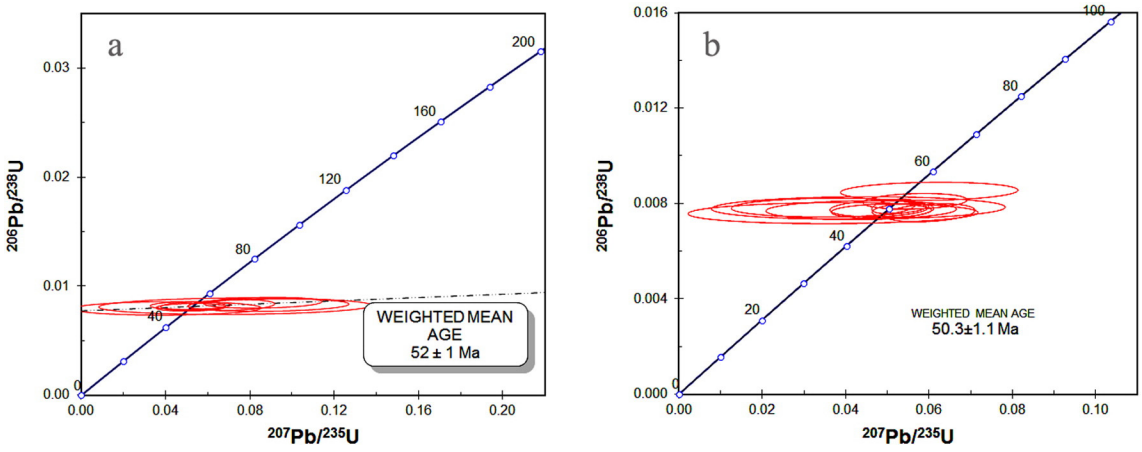

Fig. 7. Concordia diagrams displaying U–Pb data from the Kal-e-Kafi complex of quartz monzonite (a) and granite (b) (see Table1).

(Briqueu et al., 1986; Kerrich and Wyman, 1997; Pearce, 1983). The averages of the Ba/Zr and Ba/Nb ratios in the studied intrusion are 4.1 and 66.9, respectively. Therefore, they are compatible with arc magmatism.

The Kal-e-Kafi intrusive complex samples are plotted on the various tectonic discrimination diagrams and most of the samples plot in the volcanic arc field (I-type) in the Y vs. Nb, Ta vs. Yb, and Rb vs. Y + Nb diagrams (Pearce et al., 1984; Fig. 11a, b). Moreover, Gorton and Schandl (2000) suggested that Th/Ta ratio is reliable for distinguishing between different tectonic settings, especially active continental margins from oceanic arc. Therefore, the Th/Ta ratios are consistent with an active continental margin setting (Fig. 11c). In addition, samples from the studied intrusion presented in a Th/Yb vs. La/Yb (Condie, 1989) diagram plot within the field of continental arc margin settings (Fig. 11d). Finally, the K-e-Kafi complex are plotted within the fields of continental arcs and outside of post-collisional field in the Zr/TiO_2 vs. Ce/P_2O_5 (Müller and Groves, 1993, 1997) and Hf-Rb/30-Nb/4 ternary (Harris et al., 1986) tectono-magmatic discrimination diagrams (Fig. 12).

Thus in summary, the geochemical data and diagrams of the studied intrusion support an interpretation of a continental arc margin setting consistent with previous studies on the igneous rocks in the UDMA (e.g., Agard et al., 2005, 2011; Ahmadian et al., 2009; Alavi, 1994; Berberian and King, 1981; Haschke et al., 2010; Kananian et al., 2014; Sarjoughian et al., 2012). Also, voluminous magmatic rocks linearly distributed along the western margin of the Central Iranian within a number of obducted ophiolites from the collisional suture zone are geological evidence of an arc in Iran. It seems that the Eocene magmatic event may have been a consequence of complex processes involving the subduction of the Neotethys oceanic crust underneath central Iran.

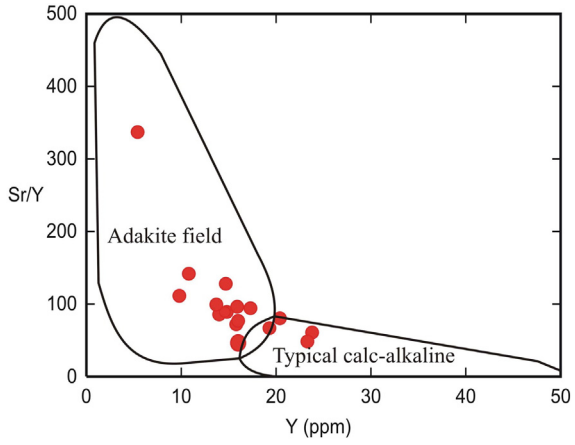

Fig. 8. Sr/Y versus Sr discrimination diagram (Defant and Drummond, 1990) of studied samples. Symbols as in Fig. 4.

6.2. Magma genesis

Here we discuss the different possibilities for generating the Kal-e-Kafi intrusive complex, from these various perspectives. Although Kal-e-Kafi intrusive complex shows typical adakitic compositional features (e.g., high Sr/Y and La/Yb), they are high in K_2O (ave: 4.24 wt.%), which is much higher than adakites from slab melting (Defant and Drummond, 1990), and is dissimilar to those of adakites derived from slab melting. They also have higher Th (ave.: 13.3 ppm) and Th/Ce (ave.: 0.23) than subducted slab-derived adakites (Wang et al., 2006a). Fig. 13 shows that high Ba/Nb ratios tend to be negatively correlated with Nb concentrations. If slab melts were directly involved in the petrogenesis of the studied rocks, a positive correlation between Ba/Nb and Nb should be observed, as adakitic magmas are thought to transport Ba and Nb into the mantle wedge (Bourdon et al., 2002; Kesson and Ringwood, 1989); therefore, it is unlikely that the studied intrusions have been derived by partial melting of a subducted oceanic slab. Also, they are characterized by bulk Earth-like Nd–Sr isotope compositions $\varepsilon Nd_{(t)} = +0.21$ to $+2.35$ and $(^{87}Sr/^{86}Sr)_i = 0.7041–0.7044$, which are inconsistent with slab-derived adakites. In addition, the age of the subducting slab becomes critical. The Arabian plate at 50 Ma is clearly too old and cold to form slab-derived adakites. Hence we conclude that the studied intrusions were unlikely to have been produced by partial melting of subducted oceanic crust.

Adakitic characteristics can also be derived by AFC processes. The following evidence indicates that these basalts did not result from AFC processes: (1) coexisting mafic rocks within the Kal-e-Kafi intrusive complex occur in very small volumes, and it is unlikely that fractionation of such small volumes of these mafic magmas could be responsible for the large volumes of granitoid rocks (see Xu et al., 2002); (2) Approximately constant Nd/Sr and high Sr concentrations of the studied intrusion suggest that the mafic magma could not evolve to form magma with adakitic compositional features by fractional crystallization of plagioclase (see Wang et al., 2004a); (3) Their Sr/Y and La/Yb ratios have no obvious correlations with MgO and SiO_2, suggesting that high Sr/Y and La/Yb ratios were inherited from a source region rather than produced by magma differentiation (see Zhao and Zhou, 2008); (4) The low Rb/Sr ratios (ave.: 0.12) rule out an origin from a mafic magma by extensive fractional crystallization (see Mirnejad et al., 2013); and (5) The Dy/Yb vs. Dy diagrams (see Gao et al., 2007; Fig. 14) indicate that the studied intrusions has not undergone fractional crystallization and reflects an end-member partial melting model. Therefore, crustal

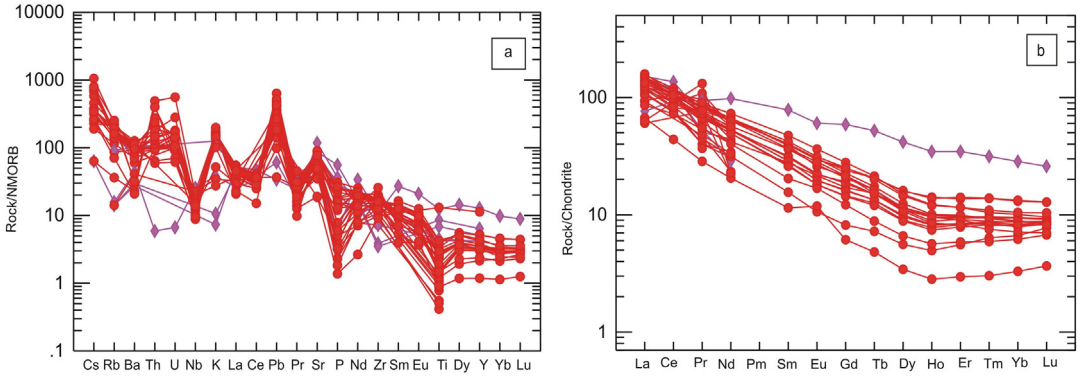

Fig. 9. NMORB-normalized trace element compositions (a) and chondrite-normalized REE patterns (b) of the Kal-e-Kafi intrusive complex (normalization factors from Sun and McDonough, 1989). Symbols as in Fig. 4.

AFC processes involving basaltic magma cannot produce the Kal-e-Kafi intrusive complex.

The relatively high SiO_2 (60–70 wt.%) contents of the studied phases of intrusion indicate that they could not be directly generated by partial melting of mantle peridotite, because low degree partial melting of mantle peridotite cannot yield acidic magmas (Green, 1980; Jahn and Zhang, 1984; Wang et al., 2006b). Anhydrous lherzolite melting experiments (Baker et al., 1995) also shows that the composition of low percentage partial melts will not be more silicic than andesites, ~55 wt.% SiO_2 at 2% melt fractions. Therefore, the studied intrusion could not have been directly derived from the partial melting of mantle peridotites (Wang et al., 2004b). In addition, partial melting of mantle peridotite cannot produce volumetrically significant felsic rocks.

Partial melting of intermediate-mafic rocks in the lower crust, heated by underplating mantle mafic magmas, is another mechanism that may yield adakitic magma (Atherton and Petford, 1993; Gromet and Silver, 1987; Petford and Atherton, 1996). Adakitic magmas formed directly from the lower crust generally have relatively low MgO contents or $Mg^{\#}$ (Rapp et al., 1991, 1999; Rapp and Watson, 1995; Sen and Dunn, 1994; Skjerlie and Patiño Doudce, 2002; Springer and Seck, 1997; Winther, 1996). They also have low Ni and V contents, high initial $^{87}Sr/^{86}Sr$ ratios (0.7071–0.7072), and low εNd values (–17.01–-18.13) similar to those of crustal rocks (Wang et al., 2004a); these characteristics indicate that the Kal-Kafi intrusive complex is not derived by lower crust melting alone. Also, their $Mg^{\#}$ values are higher than that of experimental melts of metabasalts and eclogites at pressures of 1.0–4.0 GPa (cf. Atherton and Petford, 1993; Green, 1994) implicating that they did not simply originate from partial melting of a thickened lower crust. In the Rb/Sr versus La/Ce and Rb/Sr versus Nb/U (Fig. 15a, b) diagrams (Hofmann et al., 1986; Hou et al., 2004), the compositions of the rocks from the Kal-e-Kafi intrusive complex plot between continental crust-derived melt and MORB/ slab-derived melts, with closer affinity to a crustal source.

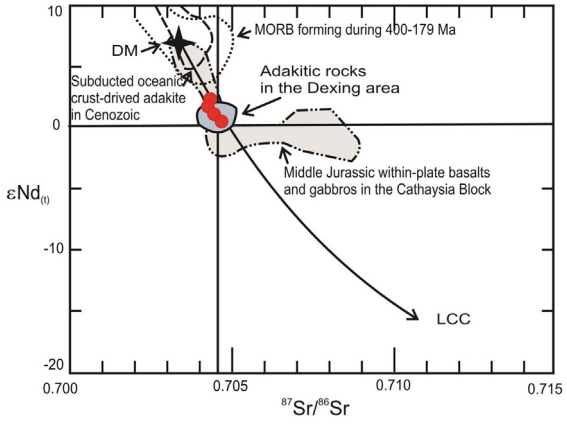

Fig. 10. Initial Sr versus εNd plot of isotopic ratios indicating the source for the magma from the Kal-e-Kafi intrusive complex. Data source are as follows: Dexing (Wang et al., 2006b); 400–179 Ma MORB are from Mahoney et al. (1998), Xu et al. (2003), Tribuzio et al. (2004) and Xu and Castillo (2004); Middle Jurassic (168–178 Ma) within-plate basalts and gabbros in the Cathaysia Block are from Li et al. (2003, 2004) and Wang et al. (2003b, 2004c); Cenozoic subducted oceanic crust-derived adakites are after Defant et al. (1992), Kay et al. (1993), and Aguillon-Robles et al. (2001); LCC (Lower continent crust); DM (Depleted mantle). Symbols as in Fig. 4.

Correspondingly, the discrimination ratios during the fractionation of magma, including Nb/Ta and Zr/Nb are moderate values in this intrusive complex (ave. 11.7 and 17.0, respectively), compared to magma derived from the enriched mantle (Nb/Ta: 17.5 and Zr/Nb: 6; Sun and McDonough, 1989), and magma derived from the lower crustal source (Nb/Ta: 11 and Zr/Nb: 25; Weaver and Tarney, 1984). Therefore, it seems that they have a hybrid genesis. Also, higher $^{87}Sr/^{86}Sr$ and lower $^{143}Nd/^{144}Nd$ relative to adakites from mantle, and lower $^{87}Sr/^{86}Sr$ and higher $^{143}Nd/^{144}Nd$ relative to adakites from lower crust melting suggest that the Kal-e-Kafi intrusions originated from partial melting of the delaminated lower continental crust (LCC), followed by interaction with the mantle peridotites.

In terms of geochemical and isotopic compositions, the Dexing adakitic porphyries (South China) exhibit relatively high Al_2O_3 (14.50–17.50 wt.%), Sr (442–2301 ppm), MgO (1.80–5.00 wt.%), Cr (30–120 ppm), and Ni (12–36 ppm) contents, with high Sr/Y (34–254), and $^{87}Sr/^{86}Sr(i)$ ratios (0.7044–0.7047) and low Yb (0.28–1.40 ppm) contents, and $\varepsilon Nd_{(t)}$ (−1.14–1.8) (Wang et al., 2006b), are similar to the Kal-e-Kafi intrusive complex (demonstrated above). This suggests that it was derived by melting of delaminated thickened lower continental crust, followed by subsequent interactions with peridotite during upward emplacement. Also, the occurrence of inherited zircon in the studied samples is consistent with a model involving partial melting of delaminating lower crust (Mirnejad et al., 2013).

A comparison of geochemical compositions of the Kal-e-Kafi intrusive complex with the Kuh Panj complex from Kerman region (Asadi et al., 2014) indicates that most of the samples of the Kuh Panj complex has lower MgO, Ni, Cr, and K_2O, but higher SiO_2 and La/Yb relative to the Kal-e-Kafi intrusive complex. The SiO_2 vs. Mg#, MgO, Ni, and Cr diagrams (Fig. 16; Lu et al., 2013) are proposed to distinguish thick lower crust derived adakite-like rocks from delaminated lower crust-derived rocks. In these diagrams, most of the Kal-e-Kafi intrusive samples plot in and near the field of delaminated lower crust-derived rocks and outside the thick lower crust-derived adakite field, but most of the Kuh Panj complex samples plot in and near to the thick lower crust-derived adakite-like field. It seems that the Kal-e-Kafi intrusions are inferred to have been derived from a delaminated lower crust. Other important differences in the Kal-e-Kafi intrusive complex and the Kuh Panj complex are in their Cu mineralization concentrations. The Kal-e-Kafi intrusive complex is presently quite small with only sub-economic porphyry

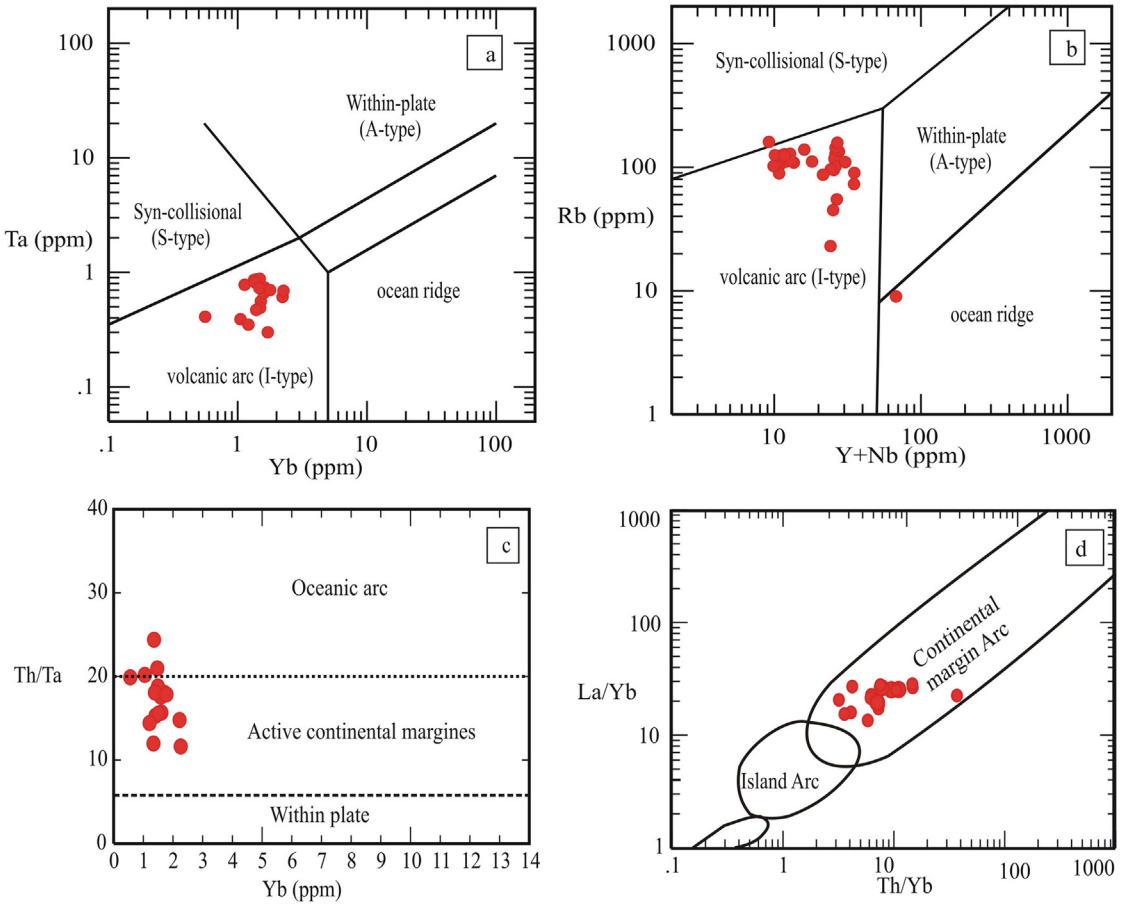

Fig. 11. Geotectonic trace-element discrimination diagrams of Pearce et al. (1984) (a, b), Gorton and Schandl (2000)(c), and Condie (1989) (d). Symbols as in Fig. 4.

systems found to date, whereas with exploration potential, especially in the coeval Eocene volcanic sequence. However, Kuh Panj complex is a giant system with economic deposits. Also the Kal-e-Kafi intrusive complex resulted from intense magmatic activity that occurred during the Eocene in response to far field subduction of the Neotethys oceanic crust underneath central Iran, but the Kuh Panj complex is coeval with the volcanoplutonic emplacement of Miocene age, suggesting post-collisional Cu mineralization. Therefore, the Kal-e-Kafi sub-economic porphyry copper complex is generally older than those of the Kuh Panj economic porphyry copper deposits.

Rapp et al. (2002) suggested that the origins of high K_2O contents is likely related to high-pressure (>1.0 GPa) melting. Therefore, the origins of relatively high K_2O contents in the studied complex are probably related to high pressure partial melting of delaminated lower crust. The melt will pass through the metasomatized mantle, as it rises towards the surface, elevating their MgO, $Mg^{\#}$, Ni, and Cr values, and decreasing Al_2O_3, Na_2O, and SiO_2 contents by the interaction between lithospheric mantle melt. Therefore the initial magmas experienced different degrees of interaction with the mantle during ascent (e.g., Atherton and Petford, 1993; Gao et al., 2004; Kepezhinskas et al., 1995; Liu et al.,

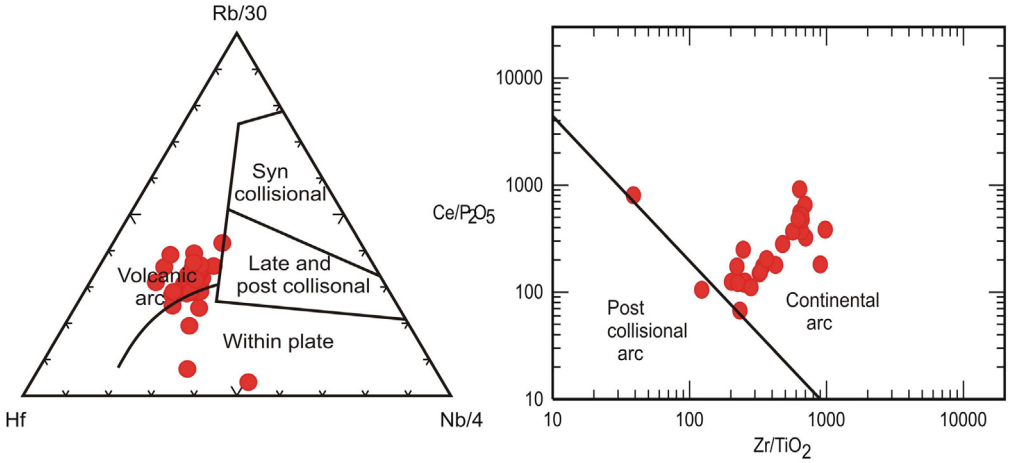

Fig. 12. Distribution of the samples in the geotectonic trace-element discrimination diagrams of Harris et al. (1986)(a) Müller and Groves (1997) (b). Symbols as in Fig. 4.

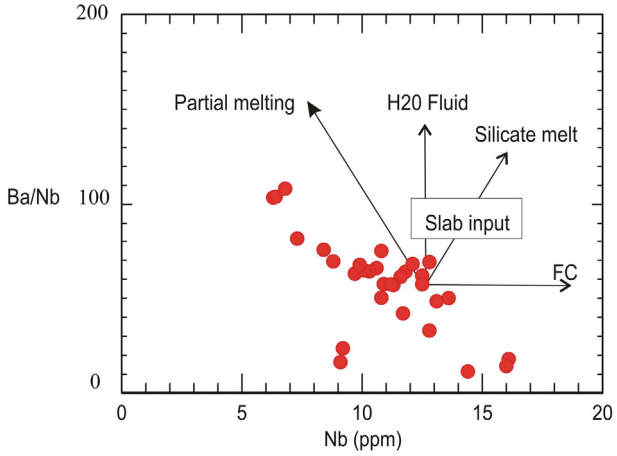

Fig. 13. Nb versus Ba/Nb diagram (Bourdon et al., 2002) with sample distribution displaying a trend consistent with a the partial melting process. Symbols as in Fig. 4.

2010; Rapp et al., 1999; Xu et al., 2002; Yogodzinski et al., 1995; Zhao and Zhou, 2008). In these scenarios, lower Mg cores than rims in the clinopyroxene (Ahmadian, 2012) indicate that they may have originated as melts of foundered lower crust with subsequent interaction of the melts with mantle peridotite (Gao et al., 2004). It must be noted that reaction between silicic melt and peridotite can modify trace element concentrations in the hybridized melts, but has a negligible effect on ratios of incompatible trace elements (cf. Rapp et al., 1999). Therefore, even if such a reaction had modified SiO_2 and MgO in some samples, it would not have a significant effect on key ratios, such as Sr/Y and La/Y (see Macpherson et al., 2006).

In the Kal-e-Kafi intrusive complex is mostly potassic with distinctly higher K_2O contents (ave.: 4.9 wt.%) and K_2O/Na_2O (ave.: 1.11). The differences in K_2O contents and K_2O/Na_2O can be explained by the presence of amphibole in the various sources. This is because amphibole is the main K-bearing mineral, having much higher K_2O than garnet and clinopyroxene in residual phases during high-pressure melting of metabasaltic rocks (e.g., Liu et al., 2010; Rapp and Watson, 1995; Sen and Dunn, 1994). The rocks are characterized by enrichment of LILE and depletion of HFSE, strongly fractionated REE pattern (ave.: La_n/Yb_n:14.31), concave-upward REE patterns, negative anomalies in Nb and Ti, coupled with positive anomalies in Sr and do not contain significant Eu anomalies. The low HREE and Y contents and the high Sr/Y and La/Yb ratios can be attributed to the presence of garnet and hornblende in the residue resulting from partial melting of their source (Atherton and Petford, 1993; Defant and Drummond, 1990). Because garnet has high partition coefficients of HREE and Y relative to LREE and Sr (Rollinson, 1993), these rocks have low Yb_n and highly variable

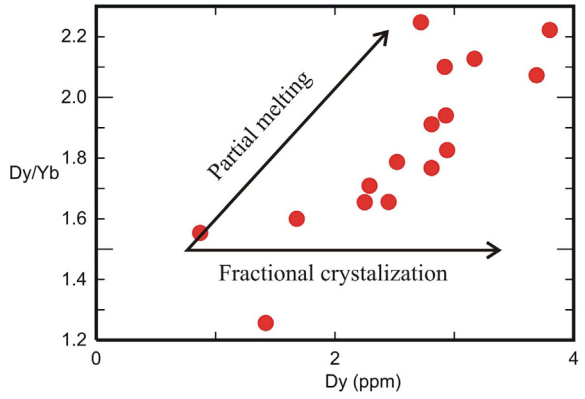

Fig. 14. La/Yb vs. La (a) and Dy/Yb vs. Yb (b) diagrams illustrating trends of fractional crystallization and versus partial melting processes. Symbols as in Fig. 4.

La_n/Yb_n ratios, suggesting that the source was a hydrous amphibole eclogite or eclogite (Zhou et al., 2006). Lack of a negative Eu anomaly indicates a lack of plagioclase fractionation from primitive magmas, suppression of plagioclase fractionation due to high magmatic water contents, and (or) high magmatic oxidation state, such that most of the Eu is present in the trivalent state and is not partitioned into fractionating plagioclase (Frey et al., 1978; Hanson, 1980; Richards et al., 2012). Furthermore, amongst the HREE, Yb, and Lu have the highest garnet-melt partition coefficients, whereas Dy and Ho have the highest hornblende-melt partition coefficients (Sisson, 1994). When garnet is the main residual phase, HREE will show strongly fractionated patterns with $Y/Yb > 10$. In contrast, when hornblende is the main residual phase, HREE will show flat patterns with $Y/Yb \approx 10$ (Ge et al., 2002). The Y/Yb ratio of the studied intrusions is 8.67 to 12.24 with the concavity of the middle REE and moderate low K/Rb (ave.: 338) indicating that residual hornblende likely existed in the source regions (Arth and Hanson, 1975; Gromet and Silver, 1987; Wang et al., 2004a).

High Sr contents and the absence of significant Eu anomalies and high Sr/Ba (ave: 2.1) preclude significant residual plagioclase in the source (Arth and Hanson, 1975; Barnes et al., 1996; Hou et al., 2004; Mo et al., 2007). The Nb and Ti negative anomalies are typical of all types of calc-alkaline magmas and they may be explained by residual hornblende and (or) Fe–Ti oxides (rutile and ilmenite) in the source of the parental magmas (Hou et al., 2004; Tatsumi, 1986), because Nb tends to be hosted in amphibole, being at equilibrium with 60–70 wt.% SiO_2 melt during partial melting (Pearce and Norry, 1979). Titanium would be hosted in rutile under hydrous mantle conditions (Tatsumi, 1986; Zhou et al., 2006). Some researchers (e.g., Gust et al., 1997; Martin, 1999; Woodhead et al., 1993) suggested that their high Sr and low Nb, Ta, and Ti contents are due to the absence of plagioclase and presence of Fe–Ti oxides in the residue in the source area of the parental magmas. Niobium and Ta contents may also be viewed as resulting from previous depletion events in the mantle source rocks and (or) the fractionation of Ti-bearing phases, such as titanite (Arjmandzadeh et al., 2011). Martin (1999) believed that the strong Nb and Ta and weak Ti negative anomalies, and absent Zr and Hf depletions, indicate residual rutile in the source, with small to moderate degrees of partial melting of eclogitic basalts at higher pressure (Gao et al., 2007; Rapp et al., 1991). These characteristics suggest that the source has residual garnet, amphibole, and possibly rutile, and thus is most likely garnet-bearing amphibole and (or) amphibole-bearing eclogite. It supports a geochemical batch melting modeling that indicates low- to medium-degree partial melting (5%–10%) of a garnet-bearing (up to 5%) basaltic amphibolite source, and lack of plagioclase as a residual component in the source for the Kal-e-Kafi intrusive complex (Ahmadian et al., 2009).

Experimental petrology and phase equilibria research (Huang and Wyllie, 1986) indicate that when the pressure is 1 GPa, the liquidus mineral of the andesitic magma system is plagioclase ± pyroxene; when >1 GPa, it is pyroxene ± garnet ± amphibole. In cases where the buried depth is more than 45 km, continental crust will be transformed into eclogite (Lai et al., 2003; Yardley and Valley, 1997). Other experimental studies (e.g., Rapp and Watson, 1995; Rapp et al., 1999, 2002, 2003) have also shown that the adakitic liquids can be produced by melting of mafic materials at pressures equivalent to crustal thicknesses of >40–50 km (i.e., >1.2 GPa), when the residual phases include garnet, garnet-amphibolite, but little or no plagioclase, most probably under eclogite facies conditions (Wang et al., 2006b). In summary, we conclude that source materials in the lower portions of thickened crust in the Kal-e-Kafi intrusive complex consisted of amphibole-bearing eclogitic and garnet-bearing amphibolitic materials with relatively high K_2O.

Wedepohl (1995) believed that in some areas with their larger thicknesses mafic granulite have transformed into eclogites with a density higher than that of lherzolite that sinks into the mantle having been detached from the lower crust. Eclogite is formed through high- to

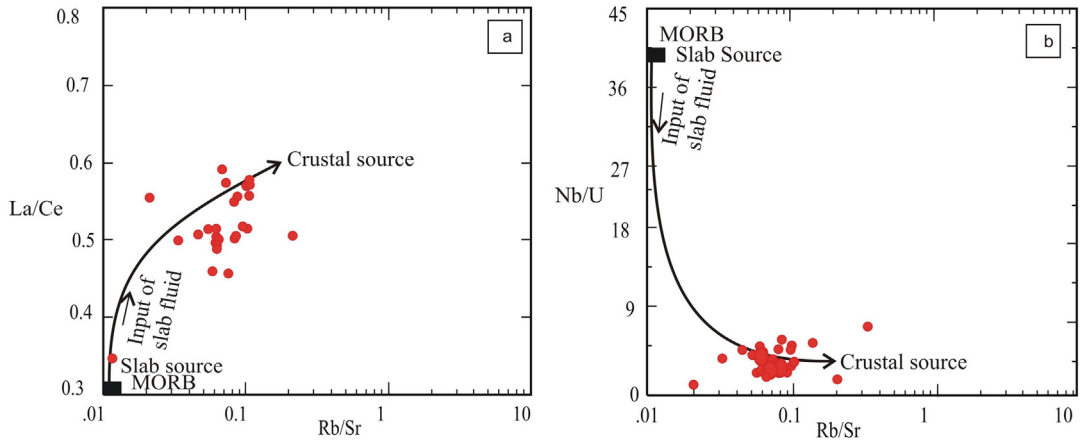

Fig. 15. Rb/Sr versus La/Ce (a) and Nb/U (b) diagrams (Hofmann et al., 1986; Hou et al., 2004) illustrating the distribution of data for the Kal-e-Kafi intrusive complex. Symbols as in Fig. 4.

ultrahigh-pressure metamorphism of basaltic rocks and has a density that is higher than peridotite by 0.2–0.4 g cm^{-3} (Rudnick and Fountain, 1995). Because of this density contrast, mafic lower continental crust (together with the underlying lithospheric mantle) can be recycled into the mantle and leads to delamination (Ducea and Saleeby, 1998; Kay and Kay, 1993; Wang et al., 2004b; Xu et al., 2002), when granulite is transformed into eclogite during crustal thickening (Gao et al., 2004; Jull and Kelemen, 2001; Kay and Kay, 1991; Wang et al., 2006b). Foundering of a dense, unstable lithospheric root into the mantle through delamination caused the replacement of eclogite by buoyant, warm asthenosphere that underwent decompressional melting to produce basaltic liquids (Dilek and Altunkaynak, 2007). When the eclogitic material was delaminated, the temperatures along the contacts between hot mantle and the eclogitic materials would have been high enough to trigger dehydration melting of amphibole-bearing eclogites at pressures >1.2 GPa (Rapp et al., 1991; Rapp and Watson, 1995; Wolf and Wyllie, 1994), which is consistent with >40 km thick Eocene central Iranian crust, forming adakitic magmas (e.g., Rapp et al., 1999, 2002). However, the present-day crustal thickness in the Kal-e-Kafi area in Central Iran is about 40 km, according to a geophysical survey by Dehghani and Makris (1983). Their data imply that the Eocene continental crust in the Kal-e-Kafi area was thicker (>40 km) than the present crust, and the continental crust, therefore, has most likely undergone a thinning process. Also, Quaternary sedimentary rocks are still preserved in the Kal-e-Kafi area, suggesting that the upper crust in this area has not undergone extensive erosion since the Eocene.

We suggest that the slower convergence rate caused crustal thickening (e.g., Shellnutt et al., 2014) and that increasing crustal thickness resulted in delamination of the lower crust and emplacement of the hot asthenosphere that generated the adakitic magmatism (Jamali and Mehrabi, 2015). This delaminated lower crust hypothesis generally involves continent–continent collision and (or) intracontinental subduction, crustal thickening, and then delamination (see Wang et al.,

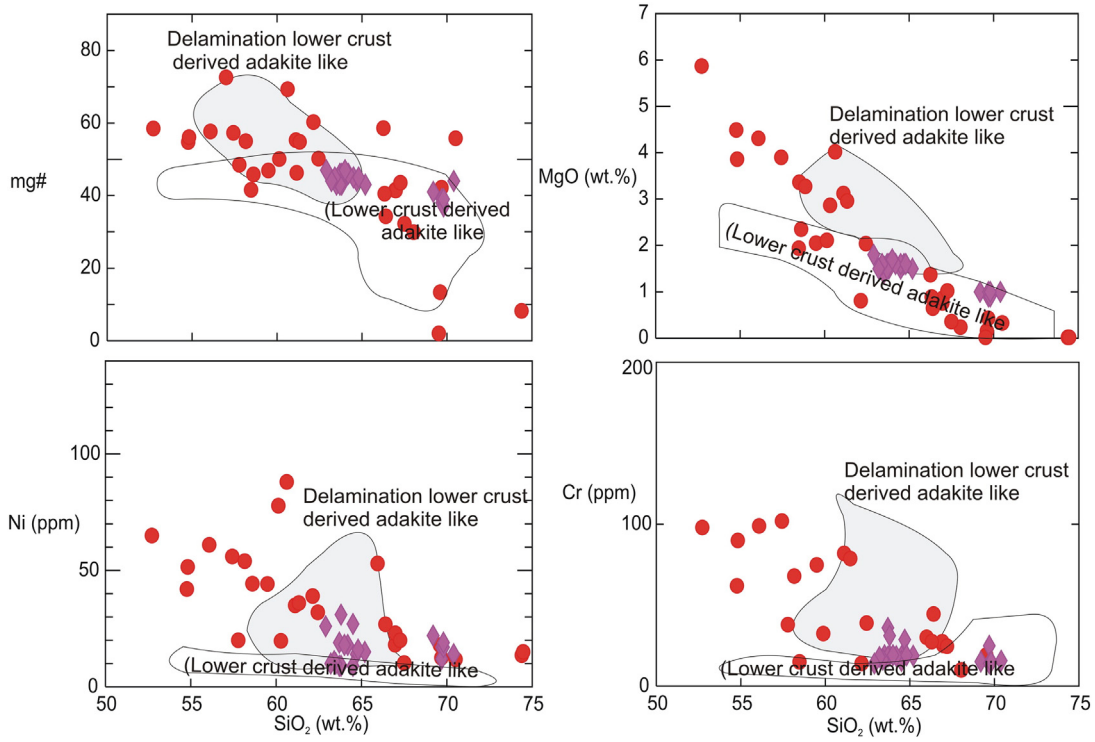

Fig. 16. Selected Harker diagrams illustrating distribution of geochemical data for the rocks of the Kal-e-Kafi complex (circle) and Kuh Panj complex (diamond). Fields of thick lower crust-derived adakite-like rocks and delaminated lower crust-derived adakite-like rocks are after Wang et al. (2006b).

2007d); following delamination or foundering, the lower crust block would have been heated by the surrounding mantle. Delamination of sub-continental mantle lithosphere with ingress of asthenospheric melts into the lower crust can cause partial melting of the metasomatized lithosphere (Brown, 2010; Richards, 2009). Potential energy that is released drives the process, as hot, low-density asthenospheric mantle replaces cold, dense lithosphere, accompanied by lithospheric thinning and increased magma production (Bird, 1979; Kay and Kay, 1991, 1993). Therefore we conclude that delamination could also explain the thinning of the Eocene crust in this part of central Iran, as a consequence of sinking of eclogitic material from the base of the lithosphere into the underlying mantle. It follows that underplating of mafic magmas related to the Neo-Tethyan subduction and subsequent Arabian–Iranian plate collision was a result of lithospheric delamination (Fig. 17). This is supported by Hatzfeld and Molnar (2010) and Shomali et al. (2011), who proposed lithospheric delamination underneath the Zagros collision zone in southwest Iran. Therefore, lithospheric thinning and possible delamination of thickened continental crust was likely responsible for the advective heat transfer that caused fusion of those metasomatized crustal segments. Subsequent reaction with the invading mantle during buoyant ascent was responsible for the petrogenesis of the Kal-e-Kafi adakitic rocks.

6.3. Implications for Cu–Au mineralization

There has been growing interest in adakitic magmatism and its relation to copper and gold mineralization in the last decade. Sillitoe (1972) studied the relationship between porphyry Cu deposits and subduction of oceanic plates and proposed that porphyry magma and the main minerogenic element metals came from the subducting oceanic plate. More recent work has emphasized the contribution of slab melts to porphyry and metallogenic metallic metals (Wang et al., 2003a). Many researchers (e.g., Defant et al., 2002; Zhang et al., 2001a, 2002) believed that slab-derived adakites are particularly prospective for Cu–Au mineralization. Mungall (2002) concluded that only slab-derived melts or supercritical fluids with high oxygen fugacity (fO_2) had the potential to generate associated epithermal and porphyry Cu–Au deposits (see also Wang et al., 2006b). They believed that slab-derived adakites have an apparently unique ability to carry this oxidizing potential up into the overlying mantle and destabilize mantle sulfides to release chalcophile Cu and Au that are mainly hosted in sulfides. Castillo (2012) also believed that adakites are more efficient in concentrating metals because they would be more oxidized and have higher sulfur and water contents, plus adakite develops better hydrothermal systems as it is more viscous and more likely to cut across older volcanic terranes (Sajona and Maury, 1998). In contrast, magmas generated by melting of underplated basaltic or gabbroic rocks in the lower crust retain the generally low fO_2 of their source and therefore are less favorable for the generation of Cu–Au deposits (Mungall, 2002; Wang et al., 2007c).

Furthermore, it has been recently recognized that some adakitic rocks derived by lower crustal melting are associated with porphyry Cu–Au deposits (e.g., Bissig et al., 2003; Hou et al., 2004; Richards, 2002; Wang et al., 2006b). As the adakitic magmas directly derived from partial melting of thickened lower crust source do not subsequently pass through the chalcophile-rich mantle peridotites source. They would fail to have the potential to generate fertile adakitic magmas to generate Cu–Au mineralization (Wang et al., 2006a,b). In contrast, adakites that ascended through the fertile mantle via delamination could have transferred notable Cu, Au, and S from the mantle to these ascending lower crustal partial melts. It is proposed that these deposits were formed from hydrous magmas derived by partial remelting of the metasomatized lithospheric roots during delamination (Richards, 2009). These melts have many of the characteristic geochemical features of arc magmas, including their relatively high water contents and oxidation states, and metal contents (Richards, 2011). Therefore, during partial melting of delaminated lower crust, adakitic magmas with high Fe_2O_3 contents interacted with the surrounding mantle peridotite, increasing the oxidation state of the mantle to beyond the NNO buffer, causing metallic sulfides in the mantle to be reincorporated into the partially molten peridotite (Mungall, 2002; Wang et al., 2006b). It seems likely that mafic magmas had to have mixed (exchanged) with the more felsic magmas, transferring amounts of sulfur, copper, and other metals to these hybrid felsic magmas and their fluids in the process (cf. Keith et al., 1997).

In subduction zones, porphyry copper deposits are generated from hydrothermal fluids exsolved from the cooling of H_2O-rich, subduction-related magmas derived from a metasomatised mantle wedge or from slab melts (e.g., Cooke et al., 2011; Richards, 2003). They yield a hot oxidized and hydrous mafic melt enriched in Cl, S, and metals (Jiang et al., 2012; Mungall, 2002; Prouteau and Scaillet, 2013; Richards, 2009). Nevertheless, the fact that not all magmas will yield fertile melts forming fertile metallogenic environments indicates that additional petrogenetic processes may be required to destabilize mantle sulfides and release chalcophile and siderophile elements (e.g., Cu–Au) into those melts (Jenner et al., 2010; Mungall, 2002; Richards, 2003, 2011).

Porphyry copper deposits are generally derived from sulfur-rich, highly oxidized magmatic systems, with oxygen fugacity (fO_2) between the nickel–nickel oxide (NNO) and magnetite–hematite oxygen (MH) buffers (Imai et al., 1993; Mungall, 2002; Oyarzun et al., 2001; Sillitoe, 1997; Wang et al., 2006b). Sulfur solubility in magmas play a key role in the formation of ore deposits. The solubility of sulfur is mainly controlled by temperature, pressure, redox conditions, melt composition, sulfur diffusion and sulfur source (Yang, 2012). This high magmatic fO_2 ultimately favors hydrothermal precipitation of large quantities of Cu and Au (& Mo in evolved felsic magmas) in direct association with magma emplacement (e.g., Müller and Groves, 1993, 1997; Wang et al., 2006a). In addition to fO_2, another important factor that controls Cu–Au mineralization must be the availability of chalcophile elements (Wang et al., 2006a), which are mainly hosted in sulfides of the mantle (Mungall, 2002; Oyarzun et al., 2001; Sillitoe, 1997). The transport of chalcophile elements from the mantle into magmas can only occur if sulfides are completely consumed during partial melting, requiring oxidation state of the mantle to have values of $\log fO_2 > FMQ + 2$ (higher than NNO buffer; Mungall, 2002; Wang et al., 2004b). Chalcophile elements (e.g., Cu and Au) are highly compatible in magmatic sulfide phases, in contrast to their general incompatible behavior in silicate and oxide minerals (Fleet et al., 1996; Liu et al., 2010), removal of them from the mantle can only occur when the

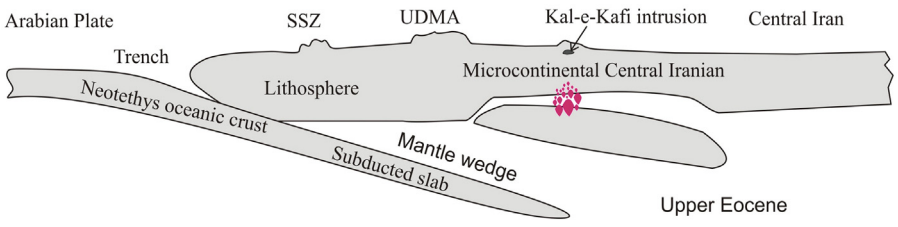

Fig. 17. Sketch showing subduction-related lithospheric delamination of the Kal-e-Kafi Intrusive Complex. SSZ and UDMA are Sanandaj–Sirjan zone and Urumieh–Dokhtar magmatic arc, respectively.

sulfide dominant in melt compositions is transformed to the sulfate-dominant under oxidized conditions (Mungall, 2002). This is supported by an empirical association between porphyry Cu–Au ore deposits and adakitic intrusions in subduction zones around the world (Gonzalez-Partida et al., 2003; Liu et al., 2010; Oyarzun et al., 2001; Thieblemont et al., 1997). Consequently, the high fO_2 would facilitate destabilization of mantle sulfides to release their Cu–Au that are mainly hosted in sulfides, and contribute to subsequent enrichment of Cu–Au in the magmas. This provides an important exploration guide for Cu–Au deposits (Liu et al., 2010). Zhang et al. (2004) also suggested that the key factor causing Cu–Au mineralization associated with adakites was the dehydration during the transformation from an amphibolite to an eclogite, which favored generation of adakitic magmas and extraction of chalcophile metals enriched in the mantle into buoyant adakitic magmas.

Sillitoe (1972) also noted that the minimally fractionated magmas are preferential for porphyry Cu–Au–Mo mineralization. The most poorly fractionated adakite magmas facilitated ore-forming materials migrate easily upwards. Since these adakite magmas are postulated to be derived from the melting of basaltic rocks, the positive to weak negative Eu anomalies actually indicate that these hybrid magmas remained quite primitive with negligible fractional crystallization of minerals (Springer and Seck, 1997) that are similar to those of these studied intrusions.

The Kal-e-Kafi porphyry Cu deposit was formed under high fO_2 similar to highly oxidized, magnetite series I-type granitoids that contain abundant primary magnetite and hematite in equilibrium with hypogene copper–iron sulfide minerals; have Fe^{3+}/Fe^{2+} ratios in biotites (green) from the studied samples plot in the field between NNO and MH oxygen buffers in the Fe^{3+}–Fe^{2+}–Mg diagram (see Ahmadian, 2012). The high H_2O and oxidation state inferred for the Kal-e-Kafi adakitic magmas, which increased SO_2/H_2S ratios (Burnham, 1979), give them considerable ore-forming potential, because they keep ore-forming components, such as Cu, Au, and S, in the melt, enabling them to partition efficiently into an exsolving fluid phase from the evolved magmas as incompatible elements (Carroll and Rutherford, 1985), and prevent the metals from partitioning into magmatic sulfide residues (Kilian and Stern, 2002). During partial melting of juvenile mafic lower crust, adakitic magmas interacted with the surrounding mantle, increasing the oxidation state of the mantle to beyond the SSO buffer, causing metallic sulfides in the mantle to be consumed (Mungall, 2002).

This means that copper enrichment in a porphyry system is likely to be caused by magmatic processes that operate entirely within the crust, resulting in copper accumulations as sulfides at the base of thicker crust (Chiaradia, 2014; Lee et al., 2012). However, copper enrichments caused by magmatic processes require a thicker arc crust (>30 km), under which the accumulation of amphibole and the fractionation of magnetite from calc-alkaline arc magmas induce sulfide saturation in magmas and consequent Cu sequestration into a sulfide melt (Chiaradia et al., 2012; Nadeau et al., 2010; Hou and Zhang, 2014). As elaborated above, the Kal-e-Kafi adakitic magmas were probably formed in the thickened continental crust setting, were related partial melting of thickened (>40 km) LCC that was then hybridized with the ascending metasomatized suprasubduction zone mantle was caused by lower crustal delamination; this scenario is favorable for the generation of porphyry Cu–Au–Mo deposits. Accordingly, we suggest that the mantle played a crucial role in generating Cu mineralization associated with the Kal-e-Kafi adakitic magmas. In conclusion, since the Kal-e-Kafi magmas were derived from the melting of basaltic rocks under high pressure and temperature, which is favorable for the enrichment of the Cu–Au ore-forming materials with the help of the abundant fluids, the adakitic magmas are capable of dissolving and carrying Cu–Au ore-forming materials, S, and fluid. When these magmas reach shallow crustal levels after they ascend through the crust quickly, failure of the surrounding rocks resulted in a rapid pressure decrease, quench cooling and solidification (porphyry generation) of the magma, and exsolution of metalliferous SO_2-bearing magmatic volatiles directly responsible for generating associated Cu-Au mineralization and associated hydrothermal altereation (e.g., Wang et al., 2003a). Importantly, inhibiting coeval volcanism impedes magma ascent through the upper crust (e.g., Gow and Walshe, 2005) and prevented the catastrophic escape of volatile phases from sulfur-rich and oxidized adakitic magmas in the hypabyssal environment, thereby facilitating the formation of porphyry various deposits (Oyarzun et al., 2001; Zhang et al., 2006).

7. Conclusions

1) The Eocene Kal-e-Kafi intrusive complex is located in the central Iran magmatic zone, which is exposed in the Anarak area of central Iran. The intrusive complex comprises as gabbro, monzonite, quartz monzonite, and granite. Excluding the gabbro, the studied intrusions have the geochemical characteristics of adakitic and shoshonitic magmas, which were emplaced in a continentally situated arc regime during the subduction of the Neo-Tethys Ocean under the Iranian Plate.
2) The studied intrusions share similar patterns of trace elements and rare earth elements, with enrichment in LREE relative to HREE, with high Sr/Y and La/Yb ratios, enrichment in LILE and Sr, depletion in HFSE, and no Eu anomalies. The trace element and Sr and Nd isotopic data demonstrate that the studied intrusions probably originated from partial melting of delaminated lower crust, which is supported by geophysical and seismological studies in this area. Lithospheric delamination involves the foundering of lower lithosphere into asthenospheric mantle, would result in deeply buried sections of the lower crust to come into contact with a relatively hot mantle; as a result partial melting begins as temperature increases. Adakitic melt hybridization during interaction with the suprasubduction zone metasomatized mantle wedge peridotites result in high siderophile and chalcophile elements and higher K than more typical lower crustal partial melts.
3) The Kal-e-Kafi magma was probably amphibole-bearing eclogitic and/or garnet-bearing amphibolite materials probably formed in the thickened continental crust setting, related to the melting of thickened (>40 km) crust. As the continental crust thickened, the lower mafic section reached pressure and temperature conditions favorable for the formation of eclogite and/or garnet-bearing amphibolite. These eclogitic materials were denser than the mantle rocks and could break away from the crust and sink, resulting in the present thinner crust in the Kal-e-Kafi area.
4) The mantle beneath the Kal-e-Kafi district played a crucial role in generating Cu–Au fertile adakitic magmas capable of dissolving and transferring plenty of Cu–Au ore-forming materials, sulfur, and fluid. Fertility is also related to highly oxidized and water-rich adakitic melts associated with interaction with the fertile mantle wedge. The rapid ascent of the adakitic magmas that were enriched in Cu and Au (and locally Mo) lead to the formation of the examples of porphyry Cu–Au deposits in this region.

Acknowledgments

We gratefully acknowledge the support by the University of Payame Noor and the Research & Development Center of the National Iranian Cu Industries Company (NICICo) for supporting this project. We acknowledge Prof. Franco Pirajno and anonymous reviewers for their constructive comments leading to important improvements in the manuscript.

References

Agard, P., Omrani, J., Jolivet, L., Mouthereau, F., 2005. Convergence history across Zagros (Iran): constraints from collisional and earlier deformation. Int. J. Earth Sci. 94, 401–419.

Agard, P., Omrani, J., Jolivet, L., Whitechurch, H., Vrielynck, B., Spakman, W., Monié, P., Meyer, B., Wortel, R., 2011. Zagros orogeny: a subduction-dominated process. Geol. Mag. 148, 692–725.

Aguillon-Robles, A., Caimus, T., Bellon, H., Maury, R.C., Cotton, J., Bourgois, J., Michaud, F., 2001. Late Miocene adakites and Nb-enriched basalts from Vizcaino Peninsula, Mexico: indicators of East Pacific Rise subduction below southern Baja California. Geology 29, 531–534.

Ahmadian, J., 2012. Geochemistry, Mineral Chemistry and Petrology of Kal-e Kafi Ore-bearing intrusive bodies, E Anarak pages, Unpublished Ph.D thesis, Tarbiat-Modaress University, Iran.

Ahmadian, J., Haschke, M., McDonald, I., Regelous, M., Ghorbani, M., Emami, M., Murata, M., 2009. High magmatic flux during Alpine-Himalayan collision: constraints from the Kal-e-Kafi complex, central Iran. Geol. Soc. Am. Bull. 121, 857–868.

Ajaji, T., Weis, D., Giret, A., Bouabdellah, M., 1998. Coeval potassic and sodic calc-alkaline series in the post-collisional Hercynian Tanncherfi intrusive complex, northeastern Morocco: geochemical, isotopic and geochronological evidence. Lithos 45, 371–393.

Alavi, M., 1994. Tectonic of the Zagros orogenic belt of Iran: new data and interpretations. Tectonophysics 229, 211–238.

Arjmandzadeh, R., Karimpour, M.H., Mazaheri, S.A., Santos, J.F., Medina, J.M., Homama, S.M., 2011. Sr–Nd isotope geochemistry and petrogenesis of the Chah-Shaljami granitoids (Lut Block, Eastern Iran). J. Asian Earth Sci. 41, 283–296.

Arth, J.G., Hanson, G.N., 1975. Geochemistry and origin of the early Precambrian crust of northeastern Minnesota. Geochim. Cosmochim. Acta 39, 325–362.

Asadi, S., Moore, F., Zarasvandi, A., 2014. Discriminating productive and barren porphyry copper deposits in the southeastern part of the central Iranian volcano-plutonic belt, Kerman region, Iran: a review. Earth Sci. Rev. 138, 25–46.

Atherton, M.P., Petford, N., 1993. Generation of sodium-rich magmas from newly underplated basaltic crust. Nature 362, 144–146.

Ayati, F., Yavuz, F., Asadi, H., Richards, J.P., Jourdane, F., 2013. Petrology and geochemistry of calc–alkaline volcanic and subvolcanic rocks, Dalli porphyry copper–gold deposit, Markazi Province, Iran. Int. Geol. Rev. 55, 158–184.

Baker, M.B., Hischmann, M.M., Ghiorso, M.S., Stolper, E.M., 1995. Compositions of near-solidus predictive melts from experiments and thermodynamic calculations. Nature 375, 308–311.

Barnes, C.G., Petersen, S.W., Kistler, R.W., Murray, R., Kay, M.A., 1996. Source and tectonic implications of tonalite–trondhjemite magmatism in the Klamath Mountain. Contrib. Mineral. Petrol. 123, 40–60.

Berberian, F., Berberian, M., 1981. Tectono–plutonic episodes in Iran. Geol. Surv. Iran 52, 566–593.

Berberian, M., King, G.C.P., 1981. Towards a paleogeography and tectonic evolution of Iran. Can. J. Earth Sci. 18, 210–265.

Bird, P., 1979. Continental delamination and the Colorado Plateau. J. Geophys. Res. 84, 7561–7571.

Bissig, T., Clark, A.H., Lee, J.K.W., 2003. Petrogenetic and metallogenetic responses to Miocene slab flattening: new constraints from the El Indio–Pascua Au–Ag–Cu belt, Chile/Argentina. Miner. Deposita 38, 844–862.

Bourdon, E., Eissen, J.P., Monzier, M., Robin, C., Martin, H., Cotton, J., Hall, M., 2002. Adakite-like lavas from Antisana Volcano (Ecuador): evidence for slab melt metasomatism beneath the Andean North Volcanic Zone. J. Petrol. 43, 199–217.

Briqueu, L., Javoy, M., Lancelot, J.R., Tatsumoto, M., 1986. Isotope geochemistry of recent magmatism in the Aegean arc: Sr, Nd, Hf, and O isotopic ratios in the lavas of Milos and Santorini-geodynamic implication. Earth Planet. Sci. Lett. 80, 41–54.

Brown, M., 2010. Melting of the continental crust during orogenesis: the thermal, rheological and compositional consequences of melt transport from lower to upper continental crust. Can. J. Earth Sci. 47, 655–694.

Burnham, C.W., 1979. Magmas and hydrothermal fluids. In: Barnes, H.L. (Ed.), Geochemistry of Hydrothermal Ore Deposits. Wiley, New York, pp. 71–136.

Carroll, M.R., Rutherford, M.J., 1985. Sulfide and sulfate saturation in hydrous silicate melts. J. Geophys. Res. 90, 601–612.

Castillo, P.R., 2006. An overview of adakite petrogenesis. Chin. Sci. Bull. 51, 257–268.

Castillo, P.R., 2012. Adakite petrogenesis. Lithos 134–135, 304–316.

Chappell, B.W., 1996. Magma mixing and the production of compositional variation within granite suites: evidence from the granites of southeastern Aust. J. Petrol. 37, 449–470.

Chiaradia, M., 2014. Copper enrichment in arc magmas controlled by overriding plate thickness. Nat. Geosci. 7, 43–46.

Chiaradia, M., Ulianov, A., Kouzmanov, K., Beate, B., 2012. Why large porphyry Cu deposits like high Sr/Y magmas? Sci. Rep. 2, 685.

Chung, S.L., Liu, D.Y., Ji, J.Q., Chu, M.F., Lee, H.Y., Wen, D.J., Lo, C.H., Lee, T.Y., Qian, Q., Zhang, Q., 2003. Adakites from continental collision zones: melting of thickened lower crust beneath southern Tibet. Geology 31, 1021–1024.

Condie, K.C., 1989. Geochemical changes in basalts and andesites across the Archean-Proterozoic boundary: identification and significance. Lithos 23, 1–18.

Cooke, D.R., Deyell, C.L., Waters, P.J., Gonzales, R.I., Zaw, K., 2011. Evidence for magmatic-hydrothermal fluids and ore-forming processes in epithermal and porphyry deposits of the Baguio District, Philippines. Econ. Geol. 106, 1399–1424.

Davidson, J., Turner, S., Handley, H., Macpherson, C., Dosseto, A., 2007. Amphibole "sponge" in arc crust? Geology 35, 787–790.

Defant, M.J., Drummond, M.S., 1990. Derivation of some modern arc magmas by melting of young subducted lithosphere. Nature 347, 662–665.

Defant, M.J., Jackson, T.E., Drummond, M.S., De Boer, J.Z., Bellon, H., Feigenson, M.D., Maury, R.C., Stewart, R.H., 1992. The geochemistry of young volcanism throughout western Panama and southeastern Costa Rica, an overview. J. Geol. Soc. Lond. 149, 569–579.

Defant, M.J., Kepezhinskas, P., Defant, M.J., Xu, J.F., Kepezhinskas, P., Wang, Q., Zhang, Q., Xiao, L., 2002. Adakites: some variations on a theme. Acta Petrol. Sin. 18, 129–142.

Dehghani, G.A., Makris, J., 1983. The gravity field and crustal structure of Iran. Neues Jb. Geol. Paläontol. Abh. 168, 215–229.

Delavari, M., Amini, S., Schmitt, A.K., McKeegan, K.D., Harrison, T.M., 2014. U–Pb geochronology and geochemistry of Bibi-Maryam pluton, eastern Iran: implication for the late stage of the tectonic evolution of the Sistan Ocean. Lithos 200–201, 197–211.

Dilek, Y., Altunkaynak, A., 2007. Cenozoic crustal evolution and mantle dynamics of post-collisional magmatism in Western Anatolia. Int. Geol. Rev. 49, 431–453.

Ding, L., Kapp, P., Yue, Y., Lai, Q., 2007. Postcollisional calc-alkaline lavas and xenoliths from the Southern Qiangtang terrane, central Tibet. Earth Planet. Sci. Lett. 254, 28–38.

Ducea, M., Saleeby, J., 1998. Crustal recycling beneath continental arcs: silica-rich glass inclusions in ultramafic xenoliths from the Sierra Nevada, California. Earth Planet. Sci. Lett. 156, 101–116.

Feeley, T.C., Cosca, M.A., 2003. Time vs. composition trends of magmatism at Sunlight volcano, Absaroka volcanic province, Wyoming. Geol. Soc. Am. Bull. 115, 714–728.

Fitton, J.G., James, D., Kempton, P.D., Ormerod, D.S., Leeman, W.P., 1988. The role of lithospheric mantle in the generation of Late Cenozoic basic magmas in the Western United States. J. Petrol. 1, 331–349.

Fleet, M.E., Crocket, J.H., Stone, W.E., 1996. Partitioning of platinum group elements (Os, Ir, Ru, Pt, Pd) and gold between sulfide liquid and basalt melt. Geochim. Cosmochim. Acta 60, 2397–2412.

Foley, S.F., Tiepolo, M., Vannucci, R., 2002. Growth of early continental crust controlled by melting of amphibolite in subduction zones. Nature 417, 637–640.

Frey, F.A., Chappell, B.W., Roy, S.D., 1978. Fractionation of rare-earth elements in the Tuolumne Intrusive Series, Sierra Nevada batholith, California. Geology 6, 239–242.

Fu, L., Wei, J., Kusky, T.M., Chen, H., Tan, J., Li, Y., Shi, W., Chen, C., Zhao, S., 2012. The Cretaceous Duimiangou adakite-like intrusion from the Chifeng region, northern North China Craton: crustal contamination of basaltic magma in an intracontinental extensional environment. Lithos 134–135, 273–288.

Gao, S., Rudnick, R.L., Yuan, H.L., Liu, X.M., Liu, Y.S., Xu, W.L., Lin, W.L., Ayers, J., Wang, X.C., Wang, Q.H., 2004. Recycling lower continental crust in the North China craton. Nature 432, 892–897.

Gao, Y., Hou, Z., Kamber, B.S., Wei, R., Meng, X., Zhao, R., 2007. Adakite-like porphyries from the southern Tibetan continental collision zones: evidence for slab melt metasomatism. Contrib. Mineral. Petrol. 153, 105–120.

Ge, X., Li, X., Chen, Z., Li, W., 2002. Geochemistry and petrogenesis of Jurassic high Sr/low Y granitoids in eastern China: constrains on crustal thickness. Chin. Sci. Bull. 47 (11).

Gonzalez-Partida, E., Levresse, G., Carrillo-Chavez, A., Cheilletz, A., Gasquet, D., Jones, D., 2003. Paleocene adakite Au–Fe bearing rocks, Mezcala, Mexico: evidence from geochemical characteristics. J. Geochem. Explor. 80, 25–40.

Gorton, M.P., Schandl, E.S., 2000. From continents to island arcs: a geochemical index of tectonic setting for arc-related and within-plate felsic o intermediate volcanic rocks. Can. Mineral. 38, 1065–1073.

Gow, P., Walshe, J.L., 2005. The role of preexisting geologic architecture in the formation of giant porphyry-related Cu ± Au deposits: examples from New Guinea and Chi. Econ. Geol. 100, 819–833.

Green, T.H., 1980. Island arc and continent-building magmatism: a review of petrogenetic models based on experimental petrology and geochemistry. Tectonophysics 63, 367–385.

Green, T.H., 1994. Experimental studies of trace element partitioning applicable to igneous petrogenesis Sedona 16 years later. Chem. Geol. 117, 1–36.

Gromet, L.P., Silver, L.T., 1987. REE variations across the Peninsular Ranges Batholith: implications for batholithic petrogenesis and crustal growth in magmtic arcs. J. Petrol. 28, 75–125.

Guo, F., Fan, W., Li, C., 2006. Geochemistry of late Mesozoic adakites from the Sulu belt, eastern China: magma genesis and implications for crustal recycling beneath continental collisional orogens. Geol. Mag. 143, 1–13.

Guo, Z., Wilson, M., Liu, J., 2007. Post-collisional adakites in South Tibet: products of partial melting of subduction-modified lower crust. Lithos 96, 205–224.

Gust, D.A., Arculus, R.A., Kersting, A.B., 1997. Aspects of magma sources and processes in the Honshu arc. Can. Mineral. 35, 347–365.

Hanson, G.N., 1980. Rare earth elements in petrogenetic studies of igneous systems. Ann. Rev. Earth Planet. Sci. 8, 371–406.

Harris, N.B.W., Pearce, J.A., Tindle, A.G., 1986. Geochemical characteristics of collision zone magmatism. In: Coward, M.P., Reis, A.C. (Eds.), Collision TectonicsGeol. Soc. Lond. Spec. Publ. 19, 67–81.

Haschke, M., Ahmadian, J., Murata, M., McDonald, I., 2010. Copper mineralization prevented by arc-root delamination during Alpine-Himalayan collision in Central Iran. Econ. Geol. 105, 855–865.

Hatzfeld, D., Molnar, P., 2010. Comparisons of the kinematics and deep structures of the Zagros and Himalaya and of the Iranian and Tibetan Plateaus, and geodynamic implications. Rev. Geophys. 48, RG2005.

Himmelberg, G.R., Loney, R.A., 1995. Characteristic and petrogenesis of Alaskan-type Ultramafic-Mafic Intrusions, Southeastern Alaska. U. S. Geol. Surv. Prof. Pap. 1564, 1–47.

Hofmann, A.W., Jochum, K.P., Seufert, M., White, W.M., 1986. Nb and Pb in oceanic basalts: new constrains on mantle evolution. Earth Planet. Sci. Lett. 79, 33–45.

Hoskin, P., Schaltegger, U., 2003. The composition of zircon and igneous and metamorphic petrogenesis. Rev. Mineral. Geochem. 53, 27–62.

Hou, Z., Zhang, H., 2014. Geodynamics and metallogeny of the eastern Tethyan metallogenic domain. Ore Geol. Rev. http://dx.doi.org/10.1016/j.oregeorev.2014.10.026.

Hou, Z.Q., Gao, Y.F., Qu, X.M., Rui, Z.Y., Mo, X.X., 2004. Origin of adakitic intrusives generated during mid-Miocene east–west extension in southern Tibet. Earth Planet. Sci. Lett. 220, 139–155.

Huang, W.L., Wyllie, P.J., 1986. Phase relationships of gabbro–tonalite–granite H_2O at 15 kbar with applications to differentiation and anatexis. Am. Mineral. 71, 301–316.
Huang, F., Li, S., Dong, F., He, Y., Chen, F., 2008. High-Mg adakitic rocks in the Dabie orogen, central China: implications for foundering mechanism of lower continental crust. Chem. Geol. 255, 1–13.
Imai, A., Listanco, E.L., Fujii, T., 1993. Petrologic and sulfur isotopic significance of highly oxidized and sulfur-rich magma of Mt. Pinatubo, Philippines. Geology 21, 585–588.
Jahangiri, A., 2007. Post-collisional Miocene adakitic volcanism in NW Iran: geochemical and geodynamic implications. J. Asian Earth Sci. 30, 433–447.
Jahn, B.M., Zhang, J.Q., 1984. Archean granulite gneisses from eastern Sino-Korean Province, China: rare earth geochemistry and tectonic implication. Contrib. Mineral. Petrol. 85, 224–243.
Jamali, H., Mehrabi, B., 2015. Relationships between arc maturity and Cu–Mo–Au porphyry andrelated epithermal mineralization at the Cenozoic Arasbaran magmatic belt. Ore Geol. Rev. 65, 481–501.
Jenner, F.E., O'Neill, H.S.T.C., Arculus, R.J., Mavrogenes, J.A., 2010. The magnetite crisis in the evolution of arc-related magmas and the initial concentration of Au, Ag and Cu. J. Petrol. 51, 2445–2464.
Jiang, Z.Q., Wang, Q., Li, Z.X., Wyman, D.A., Tang, G.J., Jia, X.H., Yang, Y.H., 2012. Late Cretaceous (ca. 90 Ma) adakitic intrusive rocks in the Kelu area, Gangdese belt (southern Tibet): slab melting and implications for Cu–Au mineralization. J. Asian Earth Sci. 53, 67–81.
Jull, M., Kelemen, P.B., 2001. On the conditions for lower crustal convective instability. J. Geophys. Res. 106, 6423–6446.
Kamber, B.S., Ewart, A., Collerson, K.D., Bruce, M.C., McDonald, G.D., 2002. Fluid-mobile trace element constraints on the role of slab melting and implications for Archaean crustal growth models. Contrib. Mineral. Petrol. 144, 38–56.
Kananian, A., Sarjoughian, F., Nadimi, A.R., Ahmadian, J., Ling, W., 2014. Geochemical characteristics of the Kuh-e Dom intrusion, Urumieh–Dokhtar Magmatic Arc (Iran): implications for source regions and magmatic evolution. J. Asian Earth Sci. 90, 137–148.
Kay, R.W., 1978. Aleutian magnesian andesites: melts from subducted Pacific Ocean crust. J. Volcanol. Geotherm. Res. 4, 117–132.
Kay, R.W., Kay, S.M., 1991. Creation and destruction of lower continental crust. Geol. Rundsch. 80, 259–278.
Kay, R.W., Kay, S.M., 1993. Delamination and delamination magmatism. Tectonophysics 219, 177–189.
Kay, S.M., Ramos, V.A., Marquez, M., 1993. Evidence in Cerro Pampa volcanic rocks of slab melting prior to ridge trench collision in southern South America. J. Geol. 101, 703–714.
Keith, J.D., Whitney, J.A., Hattori, K., Ballantyne, G.H., Christiansen, E.H., Barr, D.L., Cannan, T.M., Hook, C.J., 1997. The role of magmatic sulphides and mafic alkaline magmas in the Bingham and Tintic mining districts, Utah. J. Petrol. 38, 1679–1690.
Kelemen, P.B., Yogodzinski, G.M., Scholl, D.W., 2003. Alongstrike variation in the Aleutian island arc: genesis of high Mg# andesite and implications for continental crust. In: Eiler, J. (Ed.)The Subduction Factory, Geophys Monogr 138. Am Geophys Union, Washington, pp. 223–246.
Kepezhinskas, P.K., Defant, M.J., Drummond, M.S., 1995. Na metasomatism in the island-arc mantle by slab melt-peridotite interaction: evidence from mantle interaction: evidence from mantle xenoliths in the north Kamchatka arc. J. Petrol. 36, 1505–1527.
Kerrich, R., Wyman, D.A., 1997. Review of developments in trace-element fingerprinting of geodynamic settings and their implications for mineral exploration. Aust. J. Earth Sci. 44, 465–487.
Kesson, S.E., Ringwood, A.E., 1989. Slab-mantle interactions, sheared and refertilized garnet peridotite xenoliths-samples of Wadati-Benioff Zones? Chem. Geol. 78, 83–96.
Kilian, R., Stern, C.R., 2002. Constraints on the interaction between slab melts and the mantle wedge from adakitic glass in peridotite xenoliths. Eur. J. Mineral. 14, 25–36.
Lai, S.C., Liu, C.Y., Yi, H.S., 2003. Geochemistry and petrogenesis of Cenozoic Andesite–Dacite associations from the Hoh Xil Region, Tibetan Plateau. Int. Geol. Rev. 45, 998–1019.
Lee, C.-T.A., Luffi, P., Chin, E.J., Bouchet, R., Dasgupta, R., Morton, D.M., Le Roux, V., Yin, Q.-Z., Jin, D., 2012. Copper systematics in arc magmas and implications for crust–mantle differentiation. Science 336, 64–68.
LeMaitre, R.W., Bateman, P., Dudek, A., Keller, J., Lameyre-LeBas, M.J., Sabine, P.A., Schmid, R., Sorensen, H., Streckeisen, A., Woolley, A.R., Zanettin, B., 1989. A Classification of Igneous Rocks and Glossary of Terms. Blackwell Scientific Publications, Oxford.
Li, X.H., Chen, Z.G., Liu, D.Y., Li, W.X., 2003. Jurassic gabbro– granite–syenite suites from southern Jiangxi Province, SE China: age, origin and tectonic significance. Inter. Geol. Rev. 45, 898–921.
Li, X.H., Chung, S.L., Zhou, H.W., Lo, C.H., Liu, Y., Chen, C.H., 2004. Jurassic within-plate magmatism in southern Hunan–eastern Guangxi: 40Ar/39Ar dating, geochemistry, Sr–Nd isotopes, and implication for tectonic evolution of SE China. In: Malpas, J., Fletcher, C., Ali, J.R. (Eds.), Aspects of the Tectonic Evolution of China. Geol. Soc. Lond. Spec. Publ. 226, pp. 193–215.
Liegeois, J.P., Navez, J., Hertogen, J., Black, R., 1998. Contrasting origin of post-collisional high-K calc-alkaline and shoshonitic versus alkaline and peralkaline granitoids. The use of sliding normalization. Lithos 45, 1–28.
Liu, S.A., Li, S., He, Y., Huang, F., 2010. Geochemical contrasts between early Cretaceous ore-bearing and ore-barren high-Mg adakites in central-eastern China: implications for petrogenesis and Cu–Au mineralization. Geochim. Cosmochim. Acta 74, 7160–7178.
Lu, Y.J., Kerrich, R., McCuaig, T.C., Li, Z.X., Hart, C.J.R., Cawood, P.A., Hou, Z.Q., Bagas, L., Cliff, J., Belousova, E.A., Tang, S.H., 2013. Geochemical, Sr–Nd–Pb, and zircon Hf–O isotopic compositions of Eocene–Oligocene shoshonitic and potassic adakite-like felsic intrusions in western Yunnan, SW China: petrogenesis and tectonic implications. J. Petrol. 54, 1309–1348.
Ludwig, K.R., 2003. ISOPLOT 3.00: A Geochronological Toolkit for Microsoft Excel. Berkeley Geochronology Center, California.
Macpherson, C.G., Dreher, S.T., Thirlwall, M.F., 2006. Adakites without slab melting: high pressure differentiation of island arc magma, Mindanao, the Philippines. Earth Planet. Sci. Lett. 243, 581–593.
Mahoney, J.J., Frei, R., Tejada, M.L.G., Mo, X.X., Leat, P.T., Nagler, T.P., 1998. Tracing the Indian Ocean mantle domain through time: isotopic results from old west Indian, east Tethyan, and South Pacific seafloor. J. Petrol. 39, 1285–1306.
Martin, H., 1999. The adakitic magmas: modern analogues of Archaean granitoids. Lithos 46, 411–429.
Martin, H., Moyen, J.F., 2003. Secular changes in TTG composition: comparison with modern adakites. EGS-AGU-EUG joint meeting, Nice, April, VGP7-1FR2O-001.
Martin, H., Smithies, R.H., Rapp, R.P., Moyen, J.-F., Champion, D.C., 2005. An overview of adakite, tonalite–trondhjemite–granodiorite (TTG) and sanukitoid: relationships and some implications for crustal evolution. Lithos 79, 1–24.
Mirnejad, H., Lalonde, A.E., Obeid, M., Hassanzadeh, J., 2013. Geochemistry and petrogenesis of Mashhad granitoids: an insight into the geodynamic history of the Paleo-Tethys in northeast of Iran. Lithos 170–171, 105–116.
Mo, X., Hou, Z., Niu, Y., Dong, G., Qu, X., Zhao, Z., Yang, Z., 2007. Mantle contributions to crustal thickening during continental collision: evidence from Cenozoic igneous rocks in southern Tibet. Lithos 96, 225–242.
Moyen, J.F., 2009. High Sr/Y and La/Yb ratios: the meaning of the "adakitic signature". Lithos 112, 556–574.
Muir, R.J., Weaver, S.D., Bradshaw, J.D., Eby, G.N., Evans, J.A., 1995. Geochemistry of the Cretaceous separation point Batholith, New Zealand: granitoid magmas formed by melting of mafic lithosphere. J. Geol. Soc. Lond. 152, 689–701.
Müller, D., Groves, D.I., 1993. Direct and indirect associations between potassic igneous rocks, shoshonites and gold–copper deposits. Ore Geol. Rev. 8, 383–406.
Müller, D., Groves, D.I., 1997. Potassic Igneous Rocks and Associated Gold–Copper Mineralization. 3rd edition. Springer-Verlag, Berlin (238 pp.).
Mungall, J.E., 2002. Roasting the mantle: slab melting and the genesis of major Au and Aurich Cu deposits. Geology 30, 915–918.
Murata, M., 1993. Major and trace component analysis of Korean Institute of Energy and Resources igneous rock reference samples using X-ray fluorescence spectrometer. Res. Bull. Nat. Sci. Naruto Univ. Educ. 8, 37–49.
Nadeau, O., Williams-Jones, A.E., Stix, J., 2010. Sulphide magma as a source of metals in arc-related magmatic hydrothermal ore fluids. Nat. Geosci. 3, 501–505.
Omrani, J., Agard, P., Whitechurch, H., Benoit, M., Prouteau, G., Jolivet, L., 2008. Arc-magmatism and subduction history beneath the Zagros Mountains, Iran: a new report of adakites and geodynamic consequences. Lithos 106, 380–398.
Oyarzun, R., Marquez, A., Lillo, J., Lopez, I., Rivera, S., 2001. Giant versus small porphyry copper deposits of Cenozoic age in northern Chile: adakitic versus normal calcalkaline magmatism. Miner. Deposita 36, 794–798.
Pearce, J.A., 1982. Trace element characteristics of lavas from destructive plate boundaries. In: Thorpe, R.S. (Ed.), Andesites. Wiley, New York, pp. 525–548.
Pearce, J.A., 1983. Role of the sub-continental lithosphere in magma genesis at active continental margins. In: Hawkesworth, C.J., Norry, M.J. (Eds.), Continental Basalts and Mantle Xenoliths. Shiva, Nantwich, pp. 230–249.
Pearce, J.A., Norry, M.J., 1979. Petrogenetic implications of Ti, Zr, Y, and Nb variations in volcanic rocks. Contrib. Mineral. Petrol. 69, 33–47.
Pearce, J.A., Harris, N.B.W., Tindle, A.G., 1984. Trace element discrimination diagrams for the tectonic interpretation of granitic rocks. J. Petrol. 25, 956–983.
Peccerillo, A., Taylor, S.R., 1976. Geochemistry of Eocene calc-alkaline volcanic rocks from the Kastamonu area, Northern Turkey. Contrib. Mineral. Petrol. 58, 63–81.
Petford, N., Atherton, M., 1996. Na-rich partial melts from newly underplated basaltic crust: the cordillera Blanca Batholith, Peru. J. Petrol. 37, 1491–1521.
Prouteau, G., Scaillet, B., 2013. Experimental constraints on sulphur behaviour in subduction zones: implications for TTG and adakite production and the global sulphur cycle since the Archean. J. Petrol. 54, 183–213.
Qu, X.M., Hou, Z.Q., Li, Y.G., 2004. Melt components derived from a subducted slab in late orogenic ore-bearing porphyries in the Gangdese copper belt, southern Tibetan plateau. Lithos 74, 131–148.
Rapp, R.P., Watson, E.B., 1995. Dehydration melting of metabasalt at 8–32 kbar: implications for continental growth and crust-mantle recycling. J. Petrol. 36, 891–931.
Rapp, R.P., Watson, E.B., Miller, C.F., 1991. Partial melting of amphibolite/eclogite and the origin of Archean trondhjemites and tonalities. Precambrian Res. 51, 1–25.
Rapp, R.P., Shimizu, N., Norman, M.D., Applegate, G.S., 1999. Reaction between slab-derived melts and peridotite in the mantle wedge: experimental constraints at 38 Gpa. Chem. Geol. 160, 335–356.
Rapp, R.P., Xiao, L., Shimizu, N., 2002. Experimental constraints on the origin of potassium-rich adakite in east China. Acta Petrol. Sin. 18, 293–311.
Rapp, R.P., Shimizu, N., Norman, M.D., 2003. Growth of early continental crust by partial melting of eclogite. Nature 425, 605–609.
Richards, J.P., 2002. Discussion on 'Giant versus small porphyry copper deposits of Cenozoic age in northern Chile: adakitic versus normal calc-alkaline magmatism' by Oyarzun et al., (Miner. Deposita. 36, 794–798, 2001). Miner. Deposita 37, 788–790.
Richards, J.P., 2003. Tectono-magmatic precursors for porphyry Cu–(Mo–Au) deposit formation. Econ. Geol. 98, 1515–1533.
Richards, J.P., 2009. Post subduction porphyry Cu–Au and epithermal Au deposits: products of remelting of subduction-modified lithosphere. Geology 37, 247–250.
Richards, J.P., 2011. Magmatic to hydrothermal metal fluxes in convergent and collided margins. Ore Geol. Rev. 40, 1–26.

Richards, J.R., Kerrich, R., 2007. Adakite-like rocks: their diverse origins and questionable role in metallogenesis. Econ. Geol. 102, 537–576.
Richards, J.P., Spell, T., Rameh, E., Razique, A., Fletcher, T., 2012. High Sr/Y magmas reflect arc maturity, high magmatic water content, and porphyry Cu ± Mo ± Au potential: examples from the Tethyan Arcs of Central and Eastern Iran and Western Pakistan. Econ. Geol. 107, 295–332.
Rollinson, H., 1993. Using Geochemical Data: Evaluation, Presentation, Interpretation. Longman Scientific and Technical, New York.
Rudnick, R.L., Fountain, D.M., 1995. Nature and composition of the continental crust: a lower crustal perspective. Rev. Geophys. 33, 267–309.
Sajona, F.G., Maury, R.C., 1998. Association of adakites with gold and copper mineralization in the Philippines. C. R. Acad. Sci. 326, 27–34.
Sarjoughian, F., Kananian, A., Haschke, M., Ahmadian, J., Ling, W., Zong, K., 2012. Magma mingling and hybridization in the Kuh-e Dom pluton, Central Iran. J. Asian Earth Sci. 54–55, 49–63.
Sen, C., Dunn, T., 1994. Dehydration melting of a basaltic composition amphibolite at 1.5 and 2.0 GPa: implications for the origin of adakites. Contrib. Mineral. Petrol. 117, 394–409.
Shafiei, B., Haschke, M., Shahabpour, J., 2009. Recycling of orogenic arc crust triggers porphyry Cu mineralization in Kerman Cenozoic arc rocks, southeastern Iran. Miner. Deposita 44, 265–283.
Shahabpour, J., 2007. Island-arc affinity of the central Iranian volcanic belt. J. Asian Earth Sci. 30, 652–665.
Shannon, J.R., Walker, B.M., Carten, R.B., Geraghty, E.P., 1982. Unidirectional solidification textures and their significance in determining relative ages of intrusions at the Henderson mine, Colorado. Geology 19, 293–297.
Shellnutt, J.G., Lee, T.Y., Brookfield, M.E., Chung, S.L., 2014. Correlation between magmatism of the Ladakh Batholith and plate convergence rates during the India–Eurasia collision. Gondwana Res. 26, 1051–1059.
Shomali, Z.H., Keshvari, F., Hassanzadeh, J., Mirzaei, N., 2011. Lithospheric structure beneath the Zagros collision zone resolved by non-linear teleseismic tomography. Geophys. J. Int. 187, 394–406.
Sillitoe, R.H., 1972. A plate tectonic model for the origin of porphyry copper deposits. Econ. Geol. 67, 184–197.
Sillitoe, R.H., 1997. Characteristic and controls of the largest porphyry copper–gold and epithermal gold deposits in the circum-Pacific region. Aust. J. Earth Sci. 44, 373–388.
Sisson, T.W., 1994. Hornblende-melt trace-element partitioning measured by ion microprobe. Chem. Geol. 117, 331–334.
Skjerlie, K.P., Patiño Doudce, A.E., 2002. The fluidabsent partial melting of a zoisite-bearing quartz eclogite from 1.0 to 3.2 GPa: implications for melting in thickened continental crust and for subduction-zone processes. J. Petrol. 43, 291–314.
Springer, W., Seck, H.A., 1997. Partial fusion of basic granulites at 5 to 15 kbar: implications for the origin of TTG magmas. Contrib. Mineral. Petrol. 127, 30–45.
Stern, C.R., Kilian, R., 1996. Role of the subducted slab, mantle wedge and continental crust in the generation of adakites from the Austral Volcanic Zone. Contrib. Mineral. Petrol. 123, 263–281.
Stöcklin, J., 1968. Structural history and tectonics of Iran; a review. Am. Assoc. Pet. Geol. Bull. 52, 1229–1258.
Sun, S.S., McDonough, W.F., 1989. Chemical and isotopic systematics of oceanic basalts; implications for mantle composition and processes. In: Saunders, A.D., Norry, M.J. (Eds.), Magmatism in the Ocean Basins. Geology Society London 42, pp. 313–345.
Tatsumi, Y., 1986. Chemical characteristics of fluid phase released from a subduction lithosphere and origin of arc magma: evidence from high-pressure experiments and natural rocks. J. Volcanol. Geotherm. Res. 29, 293–309.
Thieblemont, D., Stein, G., Lescuyer, J.L., 1997. Gisements epithermaux et porphyriques: La connexion adakite. C. R. Acad. Sci. Paris 325, 103–109.
Tribuzio, R., Thirlwall, M.F., Vannucci, R., Matthew, F., 2004. Origin of the gabbro–peridotite association from the Northern Apennine Ophiolites (Italy). J. Petrol. 45, 1109–1124.
Ulmer, P., 2007. Differentiation of mantle-derived calc-alkaline magmas at mid to lower crustal levels: experimental and petrologic constraints. Period. Mineral. 76, 309–325.
Wang, Q., Zhao, Z., Xu, J., Li, X., Bao, Z., Xiong, X., Liu, Y., 2003a. Petrogenesis and metallogenesis of the Yanshanian adakite-like rocks in the Eastern Yangtze Block. Sci. China 46, 164–176.
Wang, Y.J., Fan, W.M., Guo, F., Pen, T.P., Li, C.W., 2003b. Geochemistry of Mesozoic mafic rocks adjacent to Chenzhou– Linwu fault, South China: implications for the lithospheric boundary between the Yangtze and Cathaysia Blocks. Inter. Geol. Rev. 45, 263–286.
Wang, Q., Xu, J.F., Zhao, Z.H., Bao, Z.W., Xu, W., Xiong, X.L., 2004a. Cretaceous high-potassium intrusive rocks in the Yueshan–Hongzhen area of east China: adakites in an extensional tectonic regime within a continent. Geochem. J. 38, 417–434.
Wang, Q., Zhao, Z.H., Bao, Z.W., Xu, J.F., Liu, W., Li, C.F., Bai, Z.H., Xiong, X.L., 2004b. Geochemistry and petrogenesis of the Tongshankou and Yinzu adakitic intrusive rocks and the associated porphyry copper–molybdenum mineralization in southeast Hubei, east China. Resour. Geol. 54, 137–152.
Wang, Y.J., Liao, C.L., Fan, W.M., Peng, T.P., 2004c. Early Mesozoic OIB-type alkaline basalt in central Jiangxi Province and its tectonic implications. Geochim. 33, 109–117 (in Chinese with English abstract).
Wang, Q., McDermott, F., Xu, J.F., Bellon, H., Zhu, Y.T., 2005. Cenozoic K-rich adakitic volcanic rocks in the Hohxil area, northern Tibet: lower-crustal melting in an intracontinental setting. Geology 33, 464–468.
Wang, Q., Wyman, D.A., Xu, J.F., Zhao, Z.H., Jian, P., Xiong, X.L., Bao, Z.W., Li, C.F., Bai, Z.H., 2006a. Petrogenesis of Cretaceous adakitic and shoshonitic igneous rocks in the Luzong area, Anhui Province (eastern China): implications for geodynamics and Cu–Au mineralization. Lithos 89, 424–446.
Wang, Q., Xu, J.F., Jian, P., Bao, Z.W., Zhao, Z.H., Li, C.F., Xiong, X.L., Ma, J.L., 2006b. Petrogenesis of adakitic porphyries in an extensional tectonic setting, dexing, South China: implications for the genesis of porphyry copper mineralization. J. Petrol. 47, 119–144.
Wang, Q., Wyman, A., Xu, J.F., Wan, Y.S., Li, C.F., Zi, F., Jiang, Z.Q., Qiu, H.N., Chu, Z.Y., Zhao, Z.H., Dong, Y.H., 2007a. Triassic Nb-enriched basalts, magnesian andesites, and adakites of the Qiangtang terrane (Central Tibet): evidence for metasomatism by slabderived melts in the mantle wedge. Contrib. Mineral. Petrol. 155, 473–490.
Wang, Q., Wyman, D.A., Zhao, Z.H., Xu, J.F., Bai, Z.H., Xiong, X.L., Dai, T.M., Li, C.F., Chu, Z.Y., 2007b. Petrogenesis of carboniferous adakites and Nb-enriched arc basalts in the Alataw area, northern Tianshan Range (western China): implications for Phanerozoic crustal growth in the central Asia orogenic belt. Chem. Geol. 236, 42–64.
Wang, Q., Wyman, D.A., Xu, J.F., Zhao, Z.H., Jian, P., Zi, F., 2007c. Partial melting of thickened or delaminated lower crust in the middle of Eastern China: Implications for Cu–Au mineralization. J. Geol. 115, 149–161.
Wang, Q., Wyman, D.A., Xu, J., Jian, P., Zhao, Z., Li, C., Xu, W., Ma, J., He, B., 2007d. Early Cretaceous adakitic granites in the northern Dabie Complex, central China: implications for partial melting and delamination of thickened lower crust. Geochim. Cosmochim. Acta 71, 2609–2636.
Weaver, B.L., Tarney, J., 1984. Estimating the composition of the continental crust: an empirical approach. Nature 310, 575–577.
Wedepohl, K.H., 1995. The composition of the continental crust. Geochim. Cosmochim. Acta 59, 1217–1232.
Whitney, D.L., Evans, B.W., 2010. Abbreviations for names of rock-forming minerals. Am. Mineral. 95, 185–187.
Williams, I.S., 1998. U–Th–Pb geochronology by ion microprobe. Rev. Econ. Geol. 7, 1–35.
Wilson, M., 1989. Igneous Petrogenesis: a Global Tectonic Approach. Harper Collins Academic.
Winther, K.T., 1996. An experimentally based model for the origin of tonalitic and trondhjemitic melts. Chem. Geol. 127, 43–59.
Wolf, M.B., Wyllie, P.J., 1994. Dehydration-melting of amphibolite at 10 kbar: the effects of temperature and time. Contrib. Mineral. Petrol. 115, 369–383.
Woodhead, J., Eggins, S., Gamble, J., 1993. High field strength and transition element systematics in island arc and back-arc basin basalts: evidence for multi-phase melt extraction and a depleted mantle wedge. Earth Planet. Sci. Lett. 114, 491–504.
Xiao, L., Clemens, J.D., 2007. Origin of potassic (C-type) adakite magmas: experimental and field constraints. Lithos 95, 399–414.
Xiao, L., Zhang, H.F., Clemens, J.D., Wang, Q.W., Kan, Z.Z., Wang, K.M., Ni, P.Z., Liu, X.M., 2007. Late Triassic granitoids of the eastern margin of the Tibetan Plateau: geochronology, petrogenesis and implications for tectonic evolution. Lithos 96, 436–452.
Xu, J.F., Castillo, P.R., 2004. Geochemical and Nd–Pb isotopic characteristics of the Tethyan asthenosphere: implications for the origin of the Indian Ocean mantle domain. Tectonophysics 393, 9–27.
Xu, J.F., Shinjio, R., Defant, M.J., Wang, Q., Rapp, R.P., 2002. Origin of Mesozoic adakitic intrusive rocks in the Ningzhen area of east China: partial melting of delaminated lower continental crust? Geology 30, 1111–1114.
Xu, J.F., Castillo, P.R., Chen, F.R., Niu, H.C., Yu, X.Y., Zhen, Z.P., 2003. Geochemistry of late Paleozoic mafic igneous rocks from the Kuerti area, Xinjiang, northwest China: implications for backarc mantle evolution. Chem. Geol. 193, 137–154.
Xu, Y.G., Huang, X.L., Ma, J.L., Wang, Y.B., Iizuka, Y., Xu, J.F., Wang, Q., Wu, X.Y., 2004. Crust–mantle interaction during the tectono-thermal reactivation of the North China craton: constraints from SHRIMP U–Pb zircon chronology and geochemistry of Mesozoic plutons from Western Shandong. Contrib. Mineral. Petrol. 147, 750–767.
Yakovenko, V., Chinakov, I., Kokorin, Yu, Krivyakin, B., 1981. Detailed geological prospecting in Anarak Area (Central Iran), (Kal-e-Kafi Khuni Locality). V/O Technoexport, contract No.73105.
Yang, X.M., 2012. Sulfur solubility in felsic magmas: implications for genesis of intrusion related gold mineralization. Geosci. Can. 39, 17–32.
Yardley, B.W.D., Valley, J.W., 1997. The petrologic case for a dry lower crust. J. Geophys. Res. 102, 12173–12185.
Yogodzinski, G.M., Kay, R.W., Volynets, O.N., Koloskov, A.V., Kay, S.M., 1995. Magnesian andesite in the western Aleutian Komandorsky region: implications for slab melting and processes in the mantle wedge. Geol. Soc. Am. Bull. 107, 505–519.
Zarasvandi, A., Liaghat, S., Zentilli, M., Reynolds, P.H., 2007. $^{40}Ar/^{39}Ar$ geochronology of alteration and petrogenesis of porphyry copper-related granitoids in the Darreh-Zerreshk and Ali-Abad area, central Iran. Explor. Min. Geol. 16, 11–24.
Zarasvandi, A., Liaghat, S., Lentz, D., Hossaini, M., 2013. Characteristics of mineralizing fluids of the Darreh-Zerreshk and Ali-Abad porphyry copper deposits, Central Iran, determined by fluid inclusion microthermometry. Resour. Geol. 63, 188–209.
Zarasvandi, A., Rezaei, M., Sadeghi, M., Lentz, D., Adelpour, M., Pourkaseb, H., 2015. Rare earth element signatures of economic and sub-economic porphyry copper systems in Urumieh–Dokhtar Magmatic Arc (UDMA), Iran. Ore Geol. Rev. http://dx.doi.org/10.1016/j.oregeorev.2015.01.010.
Zhang, Q., Wang, Y., Qian, Q., 2001a. The characteristics and tectonic–metallogenic significances of the Mesozoic adakitic rocks in eastern China (in Chinese). Acta Petrol. Sin. 17, 236–244.
Zhang, Q., Qian, Q., Wang, E.C., Wang, Y., Zhao, T.P., Hao, J., Guo, G.J., 2001b. Existance of East China Plateau in mid-late Yanshan period: implication from adakites (in Chinese). Sci. Geol. Sin. 36, 248–255.
Zhang, Q., Wang, Y., Liu, W., Wang, Y.L., 2002. Adakite: its characteristics and implications (in Chinese). Geol. Bull. China 2, 431–435.

Zhang, Q., Qin, K.Z., Wang, Y.L., Zhang, F.Q., Liu, H.T., Wang, Y., 2004. Study on adakite broadened to challenge the Cu and Au exploration in China (in Chinese). Acta Petrol. Sin. 20, 195–204.

Zhang, L.C., Xiao, W.J., Qin, K.Z., Ji, J.S., Zhang, Q.I., 2006. The adakite connection of the Tuwa–Yandong copper porphyry belt, eastern Tianshan, NW China: trace element and Sr–Nd–Pb isotope geochemistry. Miner. Deposita 41, 188–200.

Zhao, J.H., Zhou, M.F., 2008. Neoproterozoic adakitic plutons in the northern margin of the Yangtze Block, China: partial melting of a thickened lower crust and implications for secular crustal evolution. Lithos 104, 231–248.

Zhou, M.F., Yan, D.P., Wang, C.L., Qi, L., Kennedy, A., 2006. Subduction-related origin of the 750 Ma Xuelongbao adakitic complex (Sichuan Province, China): implications for the tectonic setting of the giant Neoproterozoic magmatic event in South China. Earth Planet. Sci. Lett. 248, 286–300.